AD-A154 464 ANGLE AVERAGED COMPTON CROSS SECTIONS FOR DEGENERATE ELECTRON GASES(U) AIR FORCE INST OF TECH WRIGHT-PATTERSON AFB OH SCHOOL OF ENGINEERING 1/1

UNCLASSIFIED J M POCHKOWSKI MAR 85 AFIT/GNE/ENP/85M-17 F/G 20/9 NL

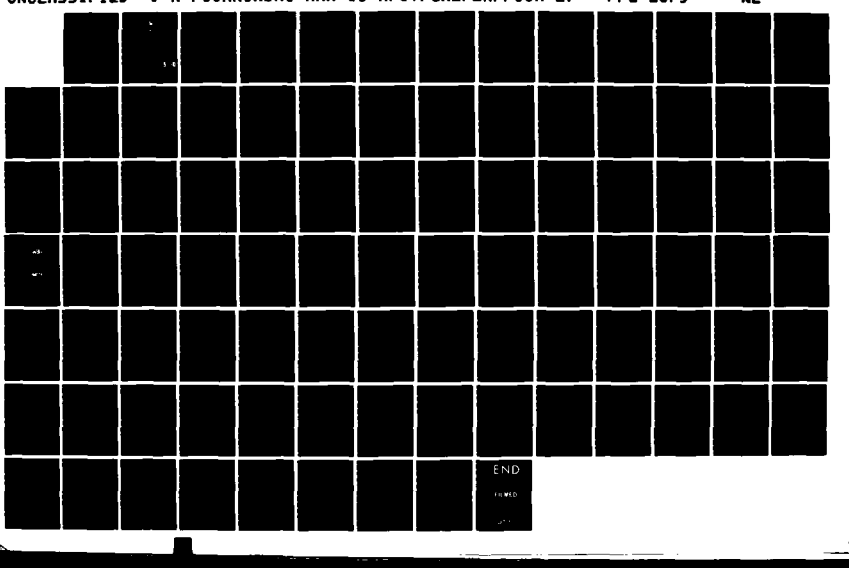

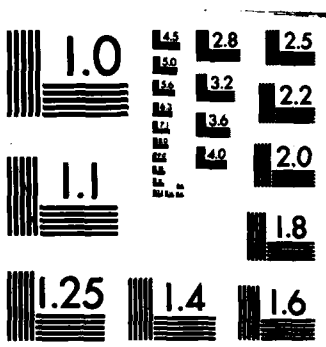

(1)

ANGLE AVERAGED COMPTON CROSS SECTIONS FOR DEGENERATE ELECTRON GASES

THESIS

Joseph M. Pochkowski
Second Lieutenant, USAF

AFIT/GNE/ENP/85M-17

DEPARTMENT OF THE AIR FORCE
AIR UNIVERSITY
AIR FORCE INSTITUTE OF TECHNOLOGY

Wright-Patterson Air Force Base, Ohio

AFIT/GNE/ENP/85M-17

ANGLE AVERAGED COMPTON CROSS SECTIONS FOR DEGENERATE ELECTRON GASES

THESIS

Joseph M. Pochkowski
Second Lieutenant, USAF

AFIT/GNE/ENP/85M-17

Approved for public release; distribution unlimited

AFIT/GNE/ENP/85M-17

ANGLE AVERAGED COMPTON CROSS SECTIONS FOR DEGENERATE ELECTRON GASES

THESIS

Presented to the Faculty of the School of Engineering
of the Air Force Institute of Technology
Air University
In Partial Fulfillment of the
Requirements for the Degree of
Master of Science in Nuclear Science

Joseph M. Pochkowski, B.S.
Second Lieutenant, USAF

March 1985

Preface

This thesis is the culmination of my efforts toward comprehending quantum statistics and its implementation in Compton scattering. It is hoped that this development can be used in transport codes to efficiently model physical phenomena without sacrificing accuracy.

I would like to thank Dr. George Nickel of Los Alamos National Laboratory for originating this work and for his constructive input. I would especially like to thank my advisor, Lieutenant Colonel William F. Bailey, for his advice, constructive criticism, and most of all his patience. Lastly, I would like to thank my wife, Cheryl, for her love and moral support during the trying times.

— Joseph M. Pochkowski

Table of Contents

List of Symbols

$D(p)$ = density of single particle states

g = spin degeneracy of the electron

V = volume of the system

h = Planck's constant

p = momentum of the electron

ϵ = kinetic energy of the electron

μ = the chemical potential

ρ = number density of electrons

m_o = rest mass of the electron

$\gamma = 1/\sqrt{1-\beta^2}$

β = ratio of electron velocity to the speed of light

k = Boltzmann's constant

T = equilibrium temperature of the electron gas

c = the speed of light

ϵ_f = the fermi energy

T_f = the fermi temperature

N = number of electrons in the system

σ_c = Compton cross section

N_s = the number of scattering centers

μ_s = collision cross section

$K(\nu \rightarrow \nu')$ = Compton scattering kernel

τ = azimuthal angle change of the photon measured in the electron rest frame

v = velocity of the electron

K_2 = second order Bessel function of the second kind

r_o = classical electron radius

$h\nu$ = the incident photon energy in the electron rest frame

$h\nu'$ = the scattered photon energy in the electron rest frame

$\sigma_{K.N.}$ = Klein-Nishina cross section

F = cumulative scattering probability

ϑ = polar angle change of the photon measured in the electron rest frame

α = the incident photon energy in the lab frame divided by the rest energy of an electron

φ = the angle between the incident photon and electron in the lab frame

α_s = the scattered photon energy in the lab frame divided by the rest energy of an electron

ζ = independent variable representing the doppler shift between rest and lab frames

ξ = independent variable representing upscatter and downscatter

a = independent variable representing the relative enrgy shift of the scattered photon

δ = angle of coordinate rotation

r = $1-\cos\vartheta$

r_{min} = the intersection in r with the surface defined by the scattered photons

q_0 = polynomial in $r_{min}^{\frac{1}{2}}$

q_1 = polynomial in $r_{min}^{\frac{1}{2}}$

h_0 = polynomial in $r_{min}^{\frac{1}{2}}$

$d(\sigma_c)$ = differential Compton cross section

α' = the incident photon energy in the rest frame divided by the rest energy of an electron

α'' = the scattered photon energy in the rest frame divided by the rest energy of an electron

R = ratio of atomic separation distance to thermal DeBroglie wavelength

List of Figures

List of Tables

Abstract

Compton scattering in dense electron gases is reviewed. The processes of Compton scattering along with a scattering inhibition factor are incorporated into the development of an analytical expression for the scattering kernel. This kernel is then used to compute angle averaged Compton cross sections for electron gases of various temperatures and number densities.

I. Introduction

Background

This report approaches the treatment of Compton scattering when the electrons are described by a degenerate distribution. In such a distribution, the electrons are at a low enough temperature and/or at a sufficiently high density so that the number of final energy states available to the scattered electrons is limited. There are a number of physical systems where the degeneracy effect is important. Electron gases present in laser fusion reactors, fusion weapons, and white dwarf stars are degenerate (4:225). The development of Compton cross sections, which could be computed quickly, for such systems would be of great use. Radiation transport computer codes that use either the P_n or S_n method require knowledge of angle averaged Compton cross sections.

Present methods of determining Compton cross sections involve interpolation from data tables acquired through numerical computations or from methods such as the Fokker-Planck approximation (5:1). The drawback to the Fokker-Planck method is that it breaks down in the relativistic regime. Although recent work indicates that an extension to relativistic distributions may be possible (8).

Current research by Dr. George Nickel of Los Alamos National Laboratory has yielded an analytic formalism for the Compton scattering kernel which describes the scattered photon distribution. The intent of this research is to extend Dr. Nickel's work to Compton scattering in degenerate electron gases, and to compute differential Compton cross sections.

Goals and Discussion

The goal of this project was to develop an analytical form of the chemical potential, incorporate it into an electron vacancy factor, and finally develop a computer code that would compute the cumulative scattering probability for degenerate gases. Time permitted the goal to be extended to the computation of angle averaged Compton cross sections. The main thrust of this research is aimed at developing accurate Compton cross sections which could be computed quickly. Therefore, it was necessary to develop as many approximations and analytic solutions as possible. These analytic expressions will eliminate lengthy numerical computations. This will hopefully decrease run times in computer codes where the Compton cross sections are used. In addition, variable transformations were used throughout the development to simplify integration. These transformations greatly simplified the surface of integration. The validation of this work is essential. Presently, no work

in the area of angle averaged Compton cross sections for degenerate systems exists and the results listed in this paper stand alone. To ensure that the computer code which generated the results was working correctly, the electron gas was treated as nondegenerate and the results compared to existing data (5:12-13). The presence of this development should be a 'tool' of considerable value to the radiation transport community. The computer code "CSP" could easily be adapted into existing codes.

Scope

This analysis is concerned with developing angle averaged Compton cross sections for degenerate electron gases and validation of the code. A particular area of application was never specifically addressed, rather it was intended that the development be generalized and its usage left to others.

II. The Electron Distribution

Fermi Distributions

The understanding and subsequent development of various parameters associated with a Fermi gas was critical in this research. The Fermi gas is described through the use of statistical mechanics. A Fermi gas receives its name because the gas consists of fermions. Fermions are a class of particles which have half integer spin and include such particles as neutrons, protons, and electrons. In this study only the electrons are examined. An area of particular interest is the distribution of fermions in the gas.

Fermions are treated as being identical and indistinguishable particles. Because of this, any fermion has an equal probability of being in any energy state. Also, fermions obey the Pauli exclusion principle which states there can only be zero or one fermion in any single particle state given by a set of quantum numbers. An equation which addresses the probability of a state being occupied can be derived by using the partition function for a grand canonical distribution, applying the above constraint, and summing over the energy states (3:197-199). The distribution function for single particle energy states is given by,

$$n(\epsilon) = \frac{1}{e^{(\epsilon-\mu)/kT} + 1} \qquad (1)$$

where

ϵ = kinetic energy of the Fermion

k = Boltzmann's constant

T = equilibrium temperature of the Fermi gas

μ = chemical potential

The chemical potential is also referred to as the Fermi energy, ϵ_F, in the limit as $T \to 0$. The chemical potential can be thought of as a mass transfer parameter and will be discussed in more detail later in this paper. At absolute zero if $\epsilon > \mu$ $n(\epsilon)$ goes to zero while if $\epsilon < \mu$ the term in the exponential goes to zero and $n(\epsilon) \to 1$. When most of the energy levels $\epsilon < \mu$ have an occupation of 1 and most of the energy levels $\epsilon > \mu$ are unoccupied, the Fermi gas is said to be degenerate. Figure 1 shows $n(\epsilon)$ versus energy when the temperature is equal to zero.

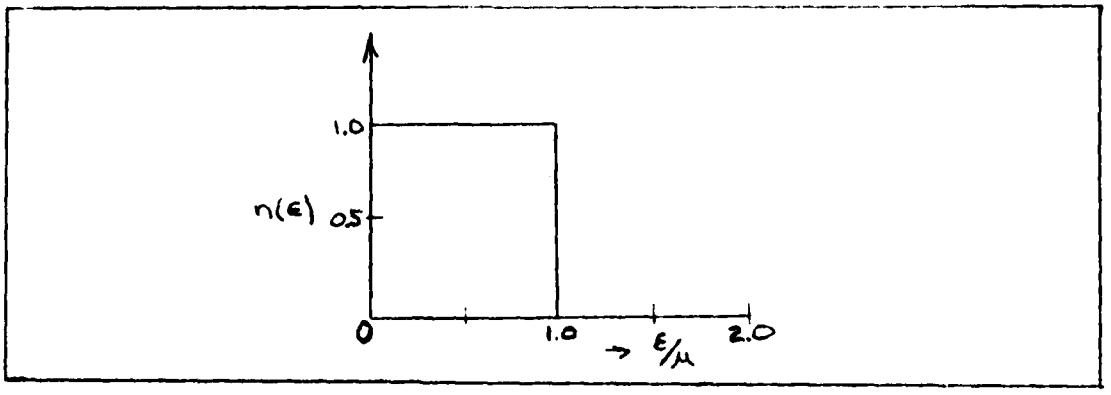

Fig. 1. Occupation of States at T=0

If T≫0 then the number of energy states available spreads out over a wider range and maximizes the total energy content of the system. Figure 2 shows n(ϵ) versus energy at temperatures much greater than zero.

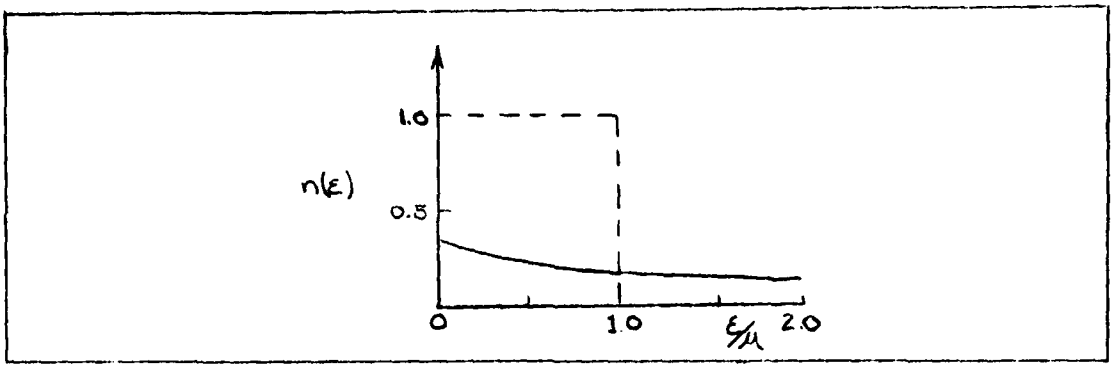

Fig. 2. Occupation of States at T>>0

Figure 3 shows the occupation of energy states as a function of temperature and speed. As will be shown later in this paper, the chemical potential is also a function of electron number density and temperature and takes on large negative values as the temperature is increased. Therefore, the exponential term in n(ϵ) goes to infinity and n(ϵ) goes to zero in the high temperature regime. Equipped with the knowledge of the occupation of energy states, the next step is to determine the Fermi distribution function.

In order to obtain the distribution of fermions in a gas, the number of available states in the system is multiplied by the probability of the energy state being occupied. The number of energy states available in a Fermi gas can be described by the quantum mechanical

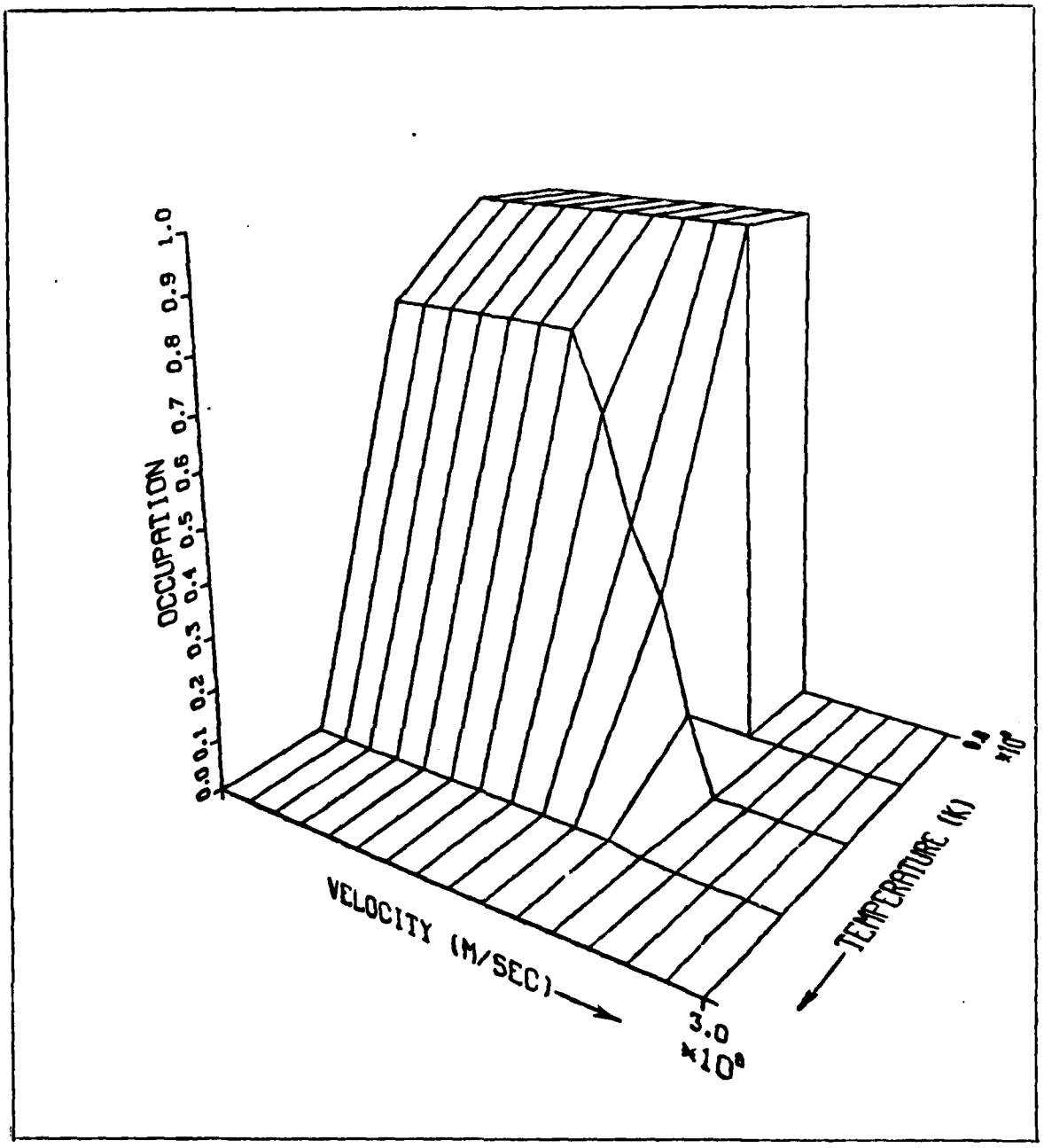

Fig. 3. Probability of Electron Energy State Occupation vs. Velocity and Temperature

results for a particle in a box. The number of states available D(p) is,

$$D(p) = \frac{4\pi g V p^2}{h^3} \qquad (2)$$

where

g = the spin degeneracy g=2s+1 (s=1/2 for Fermions)

h = Planck's constant

p = momentum

The distribution of Fermions is now

$$f(p) = \frac{4\pi g V}{h^3} \frac{p^2}{e^{(E-\mu)/kT} + 1} \qquad (3)$$

In order to understand the Fermi distribution, the behavior in the degenerate and nondegenerate limit is studied.

First, the effects of the variation of the chemical potential on the electron distribution are examined. In the case when the chemical potential is negative (non-degenerate limit), f(p) reverts back to a Maxwellian distribution. In the other limit, when the chemical potential is positive and greater than most of the kinetic energies, the gas becomes degenerate. In a degenerate gas, the accessibility to higher energy states is extremely limited. This behavior is examined in a Fermi gas as it is brought to low temperatures ($T \to 0$) or to high particle densities.

A parameter that arises from the derivation of the average energy of a Fermi gas (1:439) and is helpful in determining degeneracy is the ratio

$$R = \frac{N h^3}{V(2\pi m_o kT)^{3/2}} \qquad (4)$$

where $\frac{h}{\sqrt{2\pi m_o kT}}$ is the thermal DeBroglie wavelength and $\left(\frac{V}{N}\right)^{1/3}$ is the atomic separation distance. If the wavelength is greater than the separation distance of the particles, the wave nature is expected to be apparent. Therefore, when R is greater than or equal to one, the electron gas is degenerate.

Since, the treatment of a relativistic distribution arises in this study a relativistic form of $f(p)$ in terms of velocity was derived (Appendix E).

$$f(v) = \frac{8\pi V m_o^3}{h^3} \frac{\gamma^5 v^2}{e^{[m_o c^2(\gamma-1)-\mu]/kT}+1} \qquad (5)$$

Figures 4 and 5 show plots of this distribution F(v/vo) versus v/vo where vo is the most probable velocity associated with the distribution. A number density of 10^{25} electrons per cubic centimeter was chosen for all cases. It can be seen that the electron distribution shifts as the temperature decreases and finally exhibits the behavior of a step function characteristic of a degenerate fermi gas. When the degeneracy is nonexistent equation 5 reverts

Fermi Distribution

Maxwellian Distribution

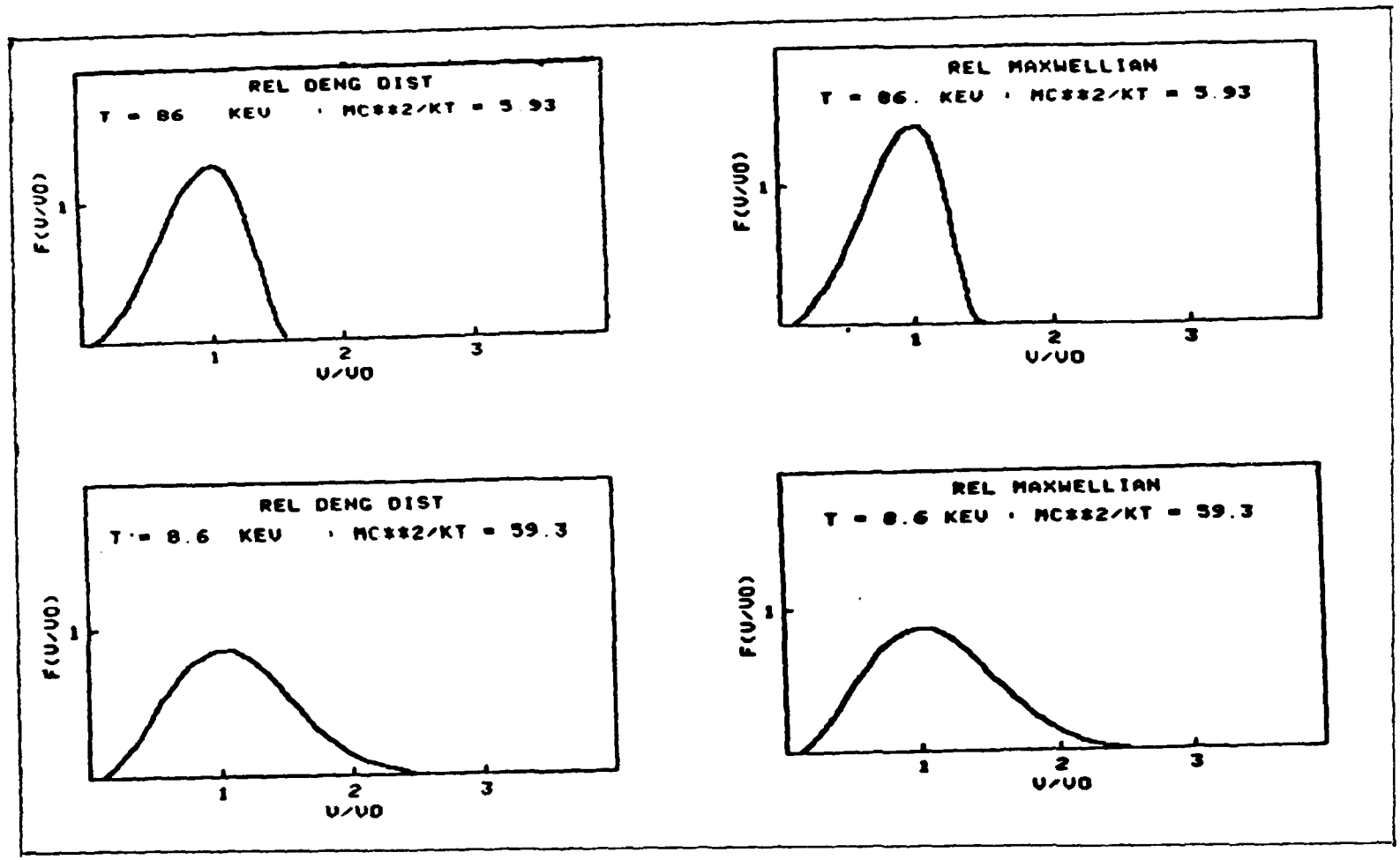

Fig. 4. Relativistic Fermi and Maxwellian Distributions (T = 86 KeV and 8.6 KeV)

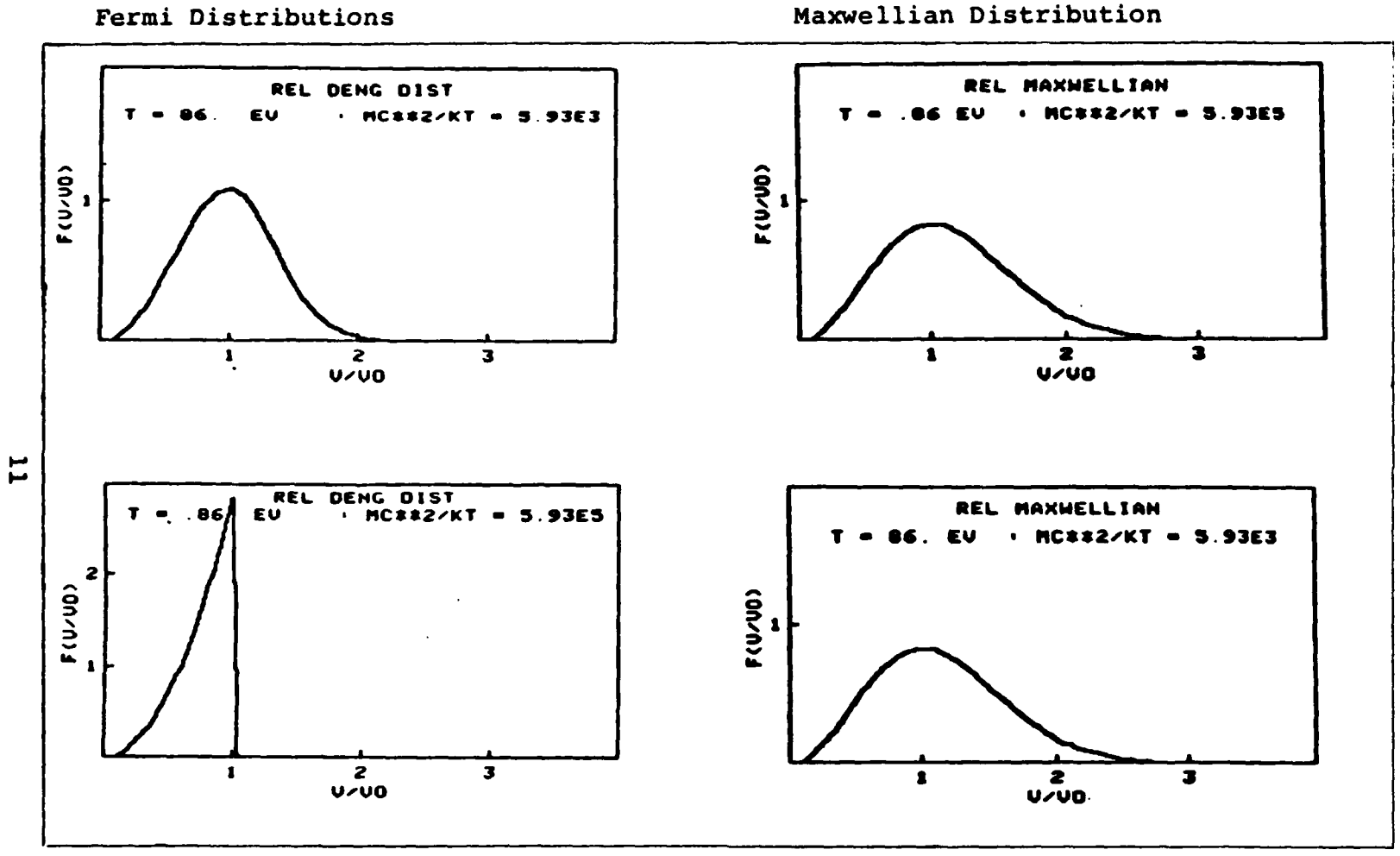

Fig. 5. Relativistic Fermi and Maxwellian Distributions (T = 86 eV and .86 eV)

to the relativistic Maxwellian. As a comparison, the plots for relativistic Maxwellians were placed adjacent to the plots of the fermi distributions. The fermi distribution was in close agreement with the relativistic Maxwellian in the nondegenerate limit. The relativistic Maxwellian distribution is given by

$$f(v) = \frac{m_o \gamma^5 e^{-m_o c^2/kT}}{4\pi c kT\, K_2\left(\frac{m_o c^2}{kT}\right)} \qquad (6)$$

where

$K_2\left(\frac{m_o c^2}{kT}\right)$ = second order Bessel function of the second kind

and can be found in reference (9). Next, an analytical form of the chemical potential is derived.

Chemical Potential

As has been shown, the chemical potential is a parameter that largely influences the behavior of the electron gas. The ability to easily compute the chemical potential presents a problem. The chemical potential can be found numerically by solving the equation,

$$N = \int_0^\infty \frac{8\pi V}{h^3} \frac{p^2 dp}{e^{(\varepsilon(p)-\mu)/kT} + 1} \qquad (7)$$

which states that the total number of particles is equal to the distribution of fermions integrated over all

momentum. This is both tedious and impractical for usage in computer codes where quick computations are a necessity. Instead, the limits in which μ is positive and negative have been examined and an analytical representation developed for each regime. When the gas is degenerative ($\mu>0$), the chemical potential (Appendix B) is given by

$$\mu = \epsilon_f \left[1 - \frac{\pi^2}{12}\left(\frac{T}{T_f}\right)^2 + \frac{\pi^4}{720}\left(\frac{T}{T_f}\right)^4 \right] \qquad (8)$$

where ϵ_f is the Fermi energy and is the value of the chemical potential at T=0. Also, the Fermi temperature is defined by the equation

$$\epsilon_f = kT_f \qquad (9)$$

In the other limit the chemical potential is

$$\mu = -kT \log \left[\frac{gV}{N} \left(\frac{m_o kT}{2\pi\hbar^2} \right)^{3/2} \right] \qquad (10)$$

Development of equations 8 and 10 is contained in Appendix C. In order to determine the accuracy of equations 8 and 10, numerical solutions were computed using equation 7. Accurate values of the numerically computed μ were obtained by doing a variable transformation and selecting a variable grid spacing for integration. Table 1 shows numerical and analytical results are in close agreement as the temperature

TABLE I

COMPARISON OF NUMERICALLY AND ANALYTICALLY COMPUTED VALUES OF THE CHEMICAL POTENTIAL (CONSTANT NUMBER DENSITY)

Number Density #/cm^3	Temperature °K	Chemical Potential Joules		Error %
		Analytic	Numerical	
10^{27}	10^{0}	5.8552×10^{-20}	5.86×10^{-20}	.08191
10^{27}	10^{1}	5.85519×10^{-20}	5.855×10^{-20}	.00325
10^{27}	10^{2}	5.8525×10^{-20}	5.8525×10^{-20}	.00000
10^{27}	10^{3}	5.877×10^{-20}	5.568×10^{-20}	.08671
10^{27}	10^{4}	-2.1675×10^{-19}	-2.073×10^{-19}	4.554
10^{27}	10^{5}	-6.933×10^{-18}	-6.9331×10^{-18}	.00144
10^{27}	10^{6}	-1.17×10^{-16}	-1.17×10^{-16}	.0000
10^{27}	10^{7}	-1.6466×10^{-15}	-1.6465×10^{-15}	.00607
10^{27}	10^{8}	-2.12×10^{-14}	-2.128×10^{-14}	.3739
10^{27}	10^{9}	-2.599×10^{-13}	-2.637×10^{-13}	1.44

is varied. Table 2 shows the same comparison yet with various number densities and temperature extremes. In table 2, the high temperature regults do not agree as closely as do the low temperature results. At high temperatures the distribution becomes relativistic and equation 10 breaks down. Any discrepancies that do arise lead to only minute effects on the distribution. Also, as the chemical potential approaches zero the analytical results start to diverge away from the numerical results. This appears to be an additional area in which the analytical representation breaks down. The parameter space of interest that this report addresses leads to values for the chemical potential which do not lie in this region.

A plot of μ/ε_f versus T/T_f is presented in figure 6 showing, as had been earlier stated, that as the temperature gets large relative to the Fermi temperature the chemical potential goes negative. The break in the curve at μ equal zero arises because of assumptions made in the development of the chemical potential. To further grasp the behavior of the chemical potential, a three-dimensional plot has been constructed. Figure 7 presents the sensitivity of the chemical potential to increases in temperature and number density. As temperature is increased and the number density held constant, the chemical potential goes to larger and larger negative values. But when the temperature is

TABLE II

COMPARISON OF NUMERICALLY AND ANALYTICALLY COMPUTED VALUES OF THE CHEMICAL POTENTIAL (VARYING DENSITY AND TEMPERATURE EXTREMES)

Number Density #/cm^3	Temperature °K	Chemical Potential Joules		Error %
		Analytic	Numerical	
10^{19}	10^{0}	2.7119×10^{-21}	2.7133×10^{-21}	.0516
10^{19}	10^{9}	-3.2354×10^{-13}	-3.267×10^{-13}	.967
10^{25}	10^{0}	2.7177×10^{-17}	2.7177×10^{-17}	.0000
10^{25}	10^{9}	-1.3289×10^{-13}	-1.3662×10^{-13}	2.73
10^{28}	10^{0}	2.7177×10^{-15}	2.7177×10^{-15}	0.000
10^{28}	10^{9}	-3.7563×10^{-14}	-4.10×10^{-14}	8.38

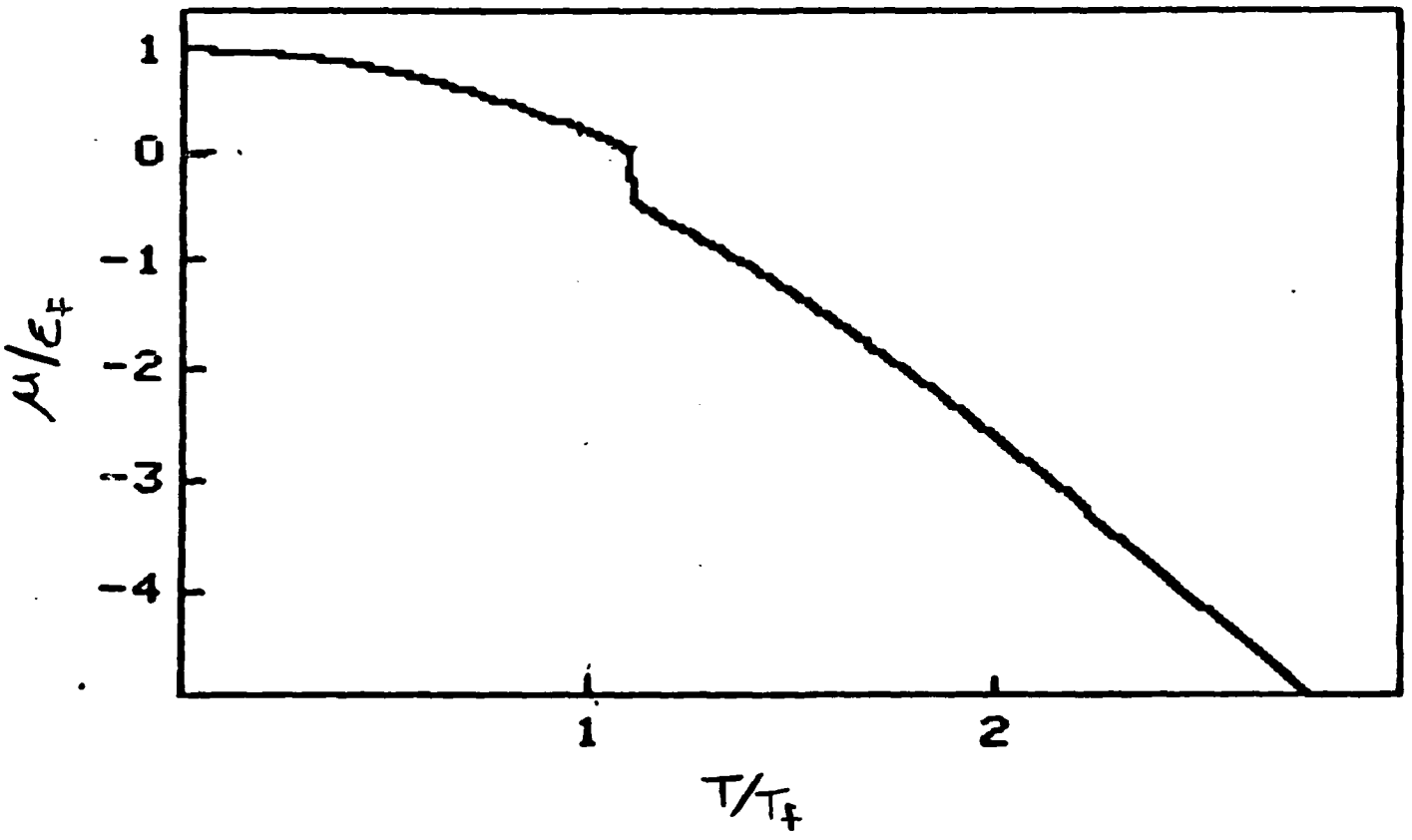

Fig. 6. Chemical Potential (Analytical) for $T<T_f$ and $T>T_f$

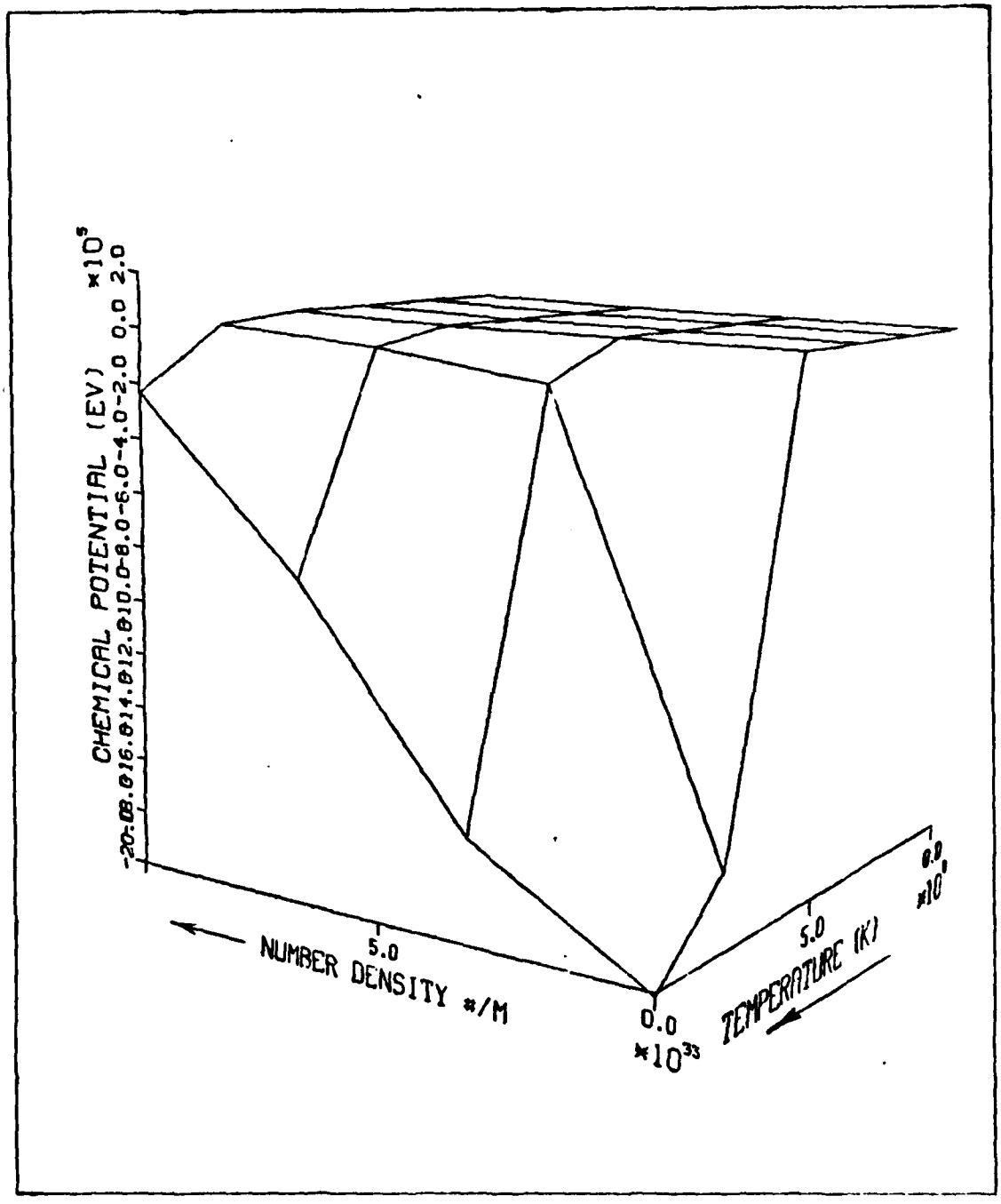

Fig. 7. Chemical Potential (Analytical) vs. Temperature and Density

large and the number density increased, the chemical potential increases. At the low temperatures, the chemical potential slightly varies with increasing number density.

III. Scattering Kernel

The Compton cross section can be decomposed into three parts.

$$\sigma_c = N_s \mu_s K(\nu \rightarrow \nu') \qquad (11)$$

where

N_s = the number of scattering centers per unit volume

μ_s = collision cross section per unit scatter

$K(\nu \rightarrow \nu')$ = the scattering kernel

The kernel is the portion of the cross section which describes the probability a photon of energy $h\nu$ will scatter to some final energy $h\nu'$. It is the dominate term in the cross section. The scattering kernel integrated over all possible scattered photon energies and angles is equal one. Therefore, a cumulative distribution function was chosen to represent the kernel.

The methodology used to develop the Compton scattering kernel for a degenerate electron gas parallels Nickel's recent work (5), but changes have been incorporated which eliminate some previous difficulties. Compton scattering is defined in terms of an incident photon scattering from an electron at rest (see figure 8).

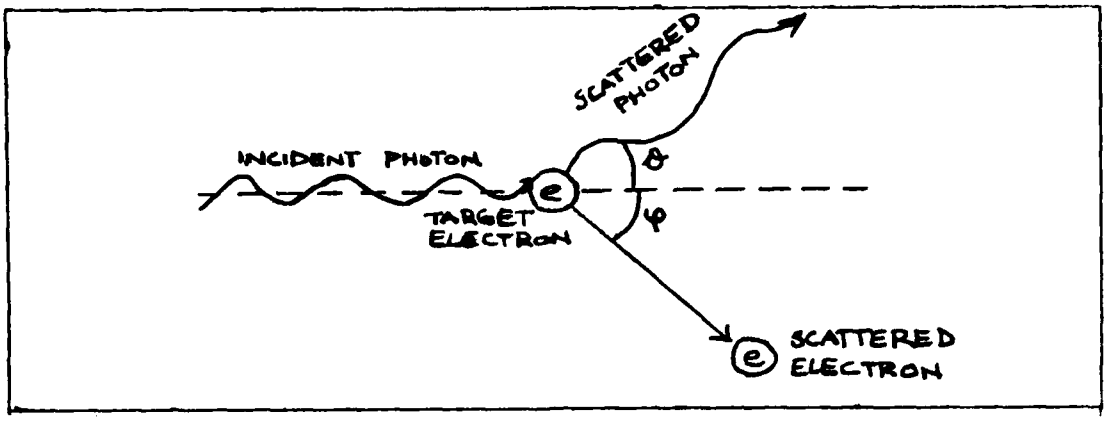

Fig. 8. Compton Scattering Geometry in the Electron Rest Frame

The Compton scattering formula,

$$h\nu' = \frac{h\nu}{1 + (1-\cos\theta)h\nu/m_o c^2} \qquad (12)$$

exhibits the characteristic that photons cannot gain energy upon scattering. But if scattering occurs between a photon and moving electron, the electron can impart some or all of its energy to the photon and increase the photon's energy. This is defined as inverse Compton scattering. The scattering kernel developed is for the case of photon scattering from a degenerate gas of free electrons.

This development begins in the laboratory frame where, the incident photon makes an angle φ with the incident electron (see figure 9). A transformation is made to the electron rest frame and Compton scattering is applied. The angles θ and τ represent a polar and azimuthal change of the scattered photon. The quantities α' and α'' are the

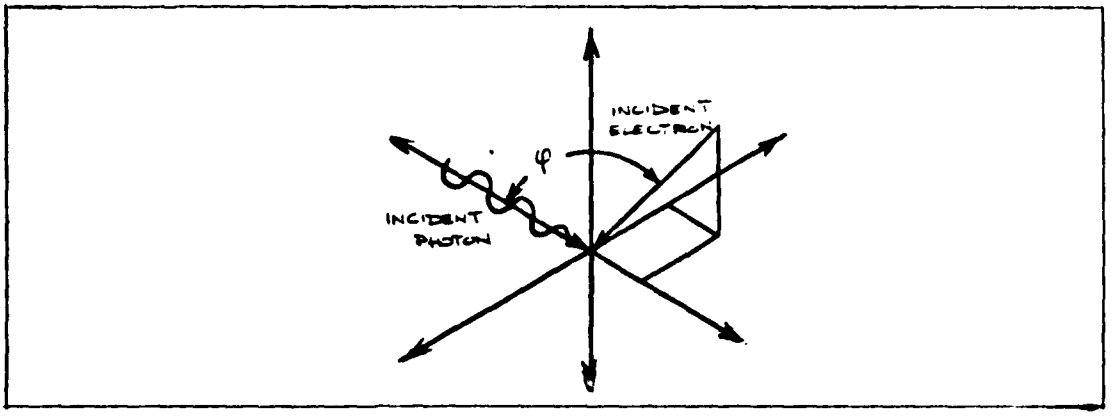

Fig. 9. Initial Scattering Geometry in the Laboratory Frame

incident and scattered photon energies in the rest frame in units of electron rest mass energy (see figure 10).

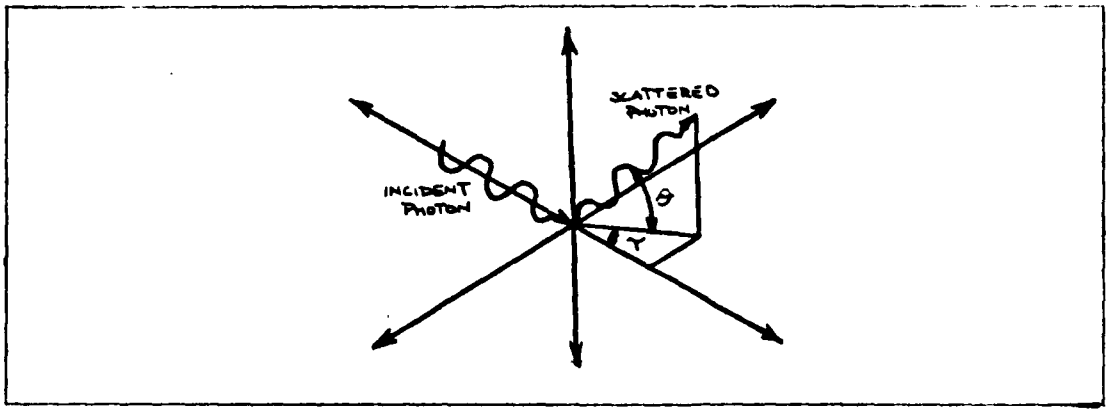

Fig. 10. Scattering Geometry in the Electron Rest Frame

Next, by transforming back to the lab frame one has,

$$\frac{\alpha_s}{\alpha} = \frac{\gamma^2(1-\beta\cos\varphi)+\beta\gamma^2\cos\theta(\cos\varphi-\beta)+\beta\gamma\sin\theta\sin\Upsilon\sin\varphi}{1+\gamma(1-\beta\cos\varphi)(1-\cos\theta)\alpha} \quad (13)$$

where α_s is now the scattered photon energy in the lab frame. The development of equation 13 is contained in

Appendix D. Equation 13 represents a surface in φ, τ, θ space and is used to determine the limits of the cumulative distribution function. The cumulative distribution function is defined as the product of the three angular distribution functions.

$$F(\alpha, \alpha_s; \beta) = \int f(\tau) d\tau \int f(\theta) d\theta \int f(\varphi) d\varphi \qquad (14)$$

$F(\alpha, \alpha_s; \beta)$ is the probability a photon of energy α will scatter to α_s by interacting with an electron of speed β. Introducing the variables ζ, ξ, a where

$$\zeta = \frac{1}{\gamma^2 \beta}\left[\frac{\alpha_s}{\alpha} - 1\right] \qquad (15)$$

$$\xi = \frac{\alpha_s}{\gamma\beta} - \beta \qquad (16)$$

$$a = \frac{\alpha_s}{\gamma} \qquad (17)$$

further simplifies equation 13, resulting in:

$$-\zeta = (1-\cos\theta)(1-a)\cos\varphi + (1-\cos\theta)\xi + \frac{1}{\gamma}\sin\theta\sin\tau\sin\varphi \qquad (18)$$

Note, that this transformation further reduces the number of independent variables from seven to five. The angular distribution functions over φ, τ, θ were selected to be

$$f(\tau) = \frac{1}{2\pi} \qquad -\pi \le \tau \le \pi \tag{19}$$

$$f(\theta) = \frac{1}{A} \frac{2 - 2(1-\alpha')(1-\cos\theta) + (1-2\alpha'+\alpha'^2)(1-\cos\theta)^2 + \alpha'(1-\cos\theta)^3}{(1+\alpha'(1-\cos\theta))^3} \tag{20}$$

$$0 \le \theta \le \pi$$

$$f(\varphi) = \frac{1}{2}\sin\varphi \qquad 0 \le \varphi \le \pi \tag{21}$$

Equation 19 assumes the polarization of the photon is unimportant. Equation 20 is the Klein-Nishina formula in the electron rest frame. A φ dependence arises in the normalization factor 'A' because of the α' term. The incident photon energy in the rest frame, α', can be defined in terms of the incident photon α in the lab frame by the equation

$$\alpha' = \alpha\gamma(1 - \beta\cos\varphi) \tag{22}$$

Thus, the φ dependence is seen. Lastly, equation 21 implies that the angle between the incident photon and electron is distributed isotropically. Next, let

$$r = (1 - \cos\theta) \tag{23}$$

and 'A' can be easily computed.

$$A = \int_0^2 dr \int_0^1 \frac{d(\cos\varphi)}{2} \frac{2 - 2(1-\alpha')r + (1-2\alpha'+\alpha'^2)r^2 + \alpha' r^3}{[1+\alpha' r]^3} \tag{24}$$

The integrals over φ, τ, r are weighted by the respective probabilities and can be regarded as the integral over a sphere of radius 'r', polar angle 'φ', and azimuthal angle 'τ' (see figure 11).

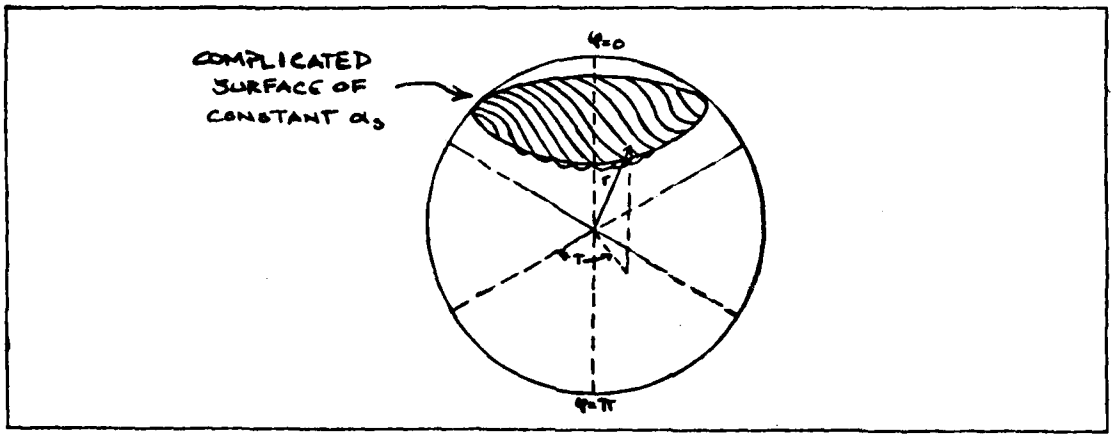

Fig. 11. Scattering Sphere over φ, τ, r Space

The integration is still difficult. Although the distribution function is now independent of τ, the boundary surface is not. A variable transform to angles φ' and τ' is made and the coordinate system is rotated by angle δ about the axis $\varphi = \pi/2$ and $\varphi = 0$ (see figures 12 and 13).

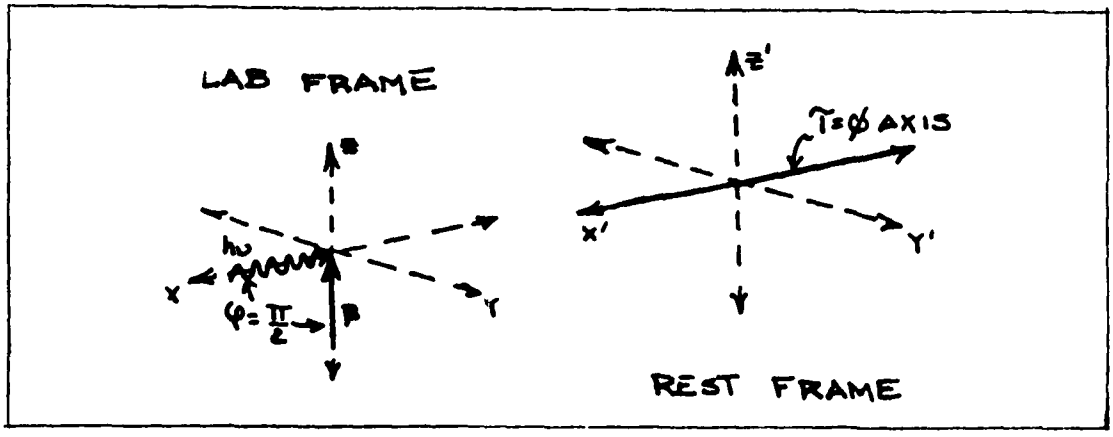

Fig. 12. Geometry Prior to Rotation

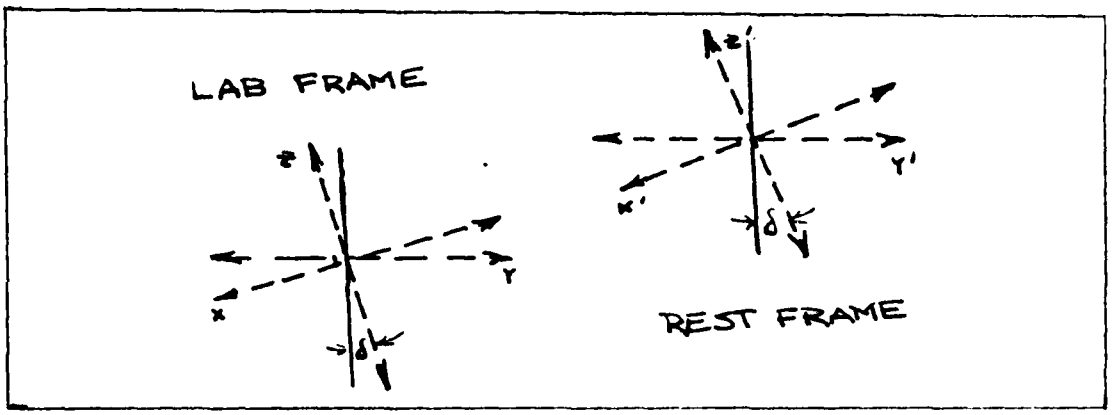

Fig. 13. Geometry After Rotation

The terms for $\cos\varphi$ and $\sin\varphi \sin\tau$ are substituted by making use of the identity (5:6)

$$\cos\varphi = \cos\varphi'\cos\delta - \sin\varphi'\sin\tau'\sin\delta \qquad (25)$$

$$\sin\varphi\sin\tau = \cos\varphi'\sin\delta + \sin\varphi'\sin\tau'\cos\delta \qquad (26)$$

where $\sin\delta$ and $\cos\delta$ are chosen as

$$\sin\delta = \frac{\sqrt{2r-r^2}}{\delta\sqrt{2r(1-\beta^2)+r^2(\beta^2-a^2)}} \qquad (27)$$

$$\cos\delta = \frac{r(1-a)}{\sqrt{2r(1-\beta^2)+r^2(\beta^2-a^2)}} \qquad (28)$$

Equation 18 reduces to

$$-\zeta = \sqrt{2r(1-\beta^2)+r^2(\beta^2-a^2)}\cos\varphi' + r\xi \qquad (29)$$

The surface is simplified but the distribution function $F(\alpha,\alpha_3;\beta)$ is complicated. Fortunately, some of the

integrals contain odd functions integrated over even intervals and are eliminated. The transformations known as 'shearing transformations' used to obtain equation 29 greatly simplify integration. Figure 14 shows the surface in space prior to and after the shearing transformation. Next, the value of 'r' at the intersection of the surface at $\varphi = 0$ or π is defined as 'rmin'. Rmin is found by solving equation 13 for its minimum value.

$$r_{min} = \frac{(1-\beta-\xi_1\zeta)^2 - \sqrt{1+\beta^2-\xi_1^2\zeta^2 - \zeta^2(\alpha^2+\xi_1^2-\beta^2)}}{\alpha^2+\xi_1^2-\beta^2} \quad [\alpha^2+\xi_1^2 \neq \beta^2] \quad (30)$$

$$r_{min} = \frac{\zeta^2}{2(\alpha^2+\xi_1^2-\beta^2)} \quad [\alpha^2+\xi_1^2 = \beta^2] \quad (31)$$

In addition, the photons can scatter over the range specified by solving the quadratic in equation 13 for α_s.

α_{min} and α_{max} are given by

$$\alpha_{s\ \substack{min\\max}} = \alpha \frac{1-\beta^2+2\gamma\alpha}{(\frac{1}{\gamma}+2\alpha)^2-\beta^2\alpha^2} \left\{ 1 \pm \sqrt{\frac{1-\frac{1}{\gamma^2}\left[(\frac{1}{\gamma}+2\alpha)^2-\beta^2\alpha^2\right]}{[1+\beta^2+2\gamma\alpha]^2}} \right\} \quad (32)$$

The limits on cos φ_1' and cos φ_2' when z<0 are

$$\cos\varphi_2' = -1 \quad (33)$$

$$\cos\varphi_1' = (\zeta+r\xi_1)/\sqrt{2r(1-\beta^2)+r^2(\beta^2-\alpha^2)} \quad (34)$$

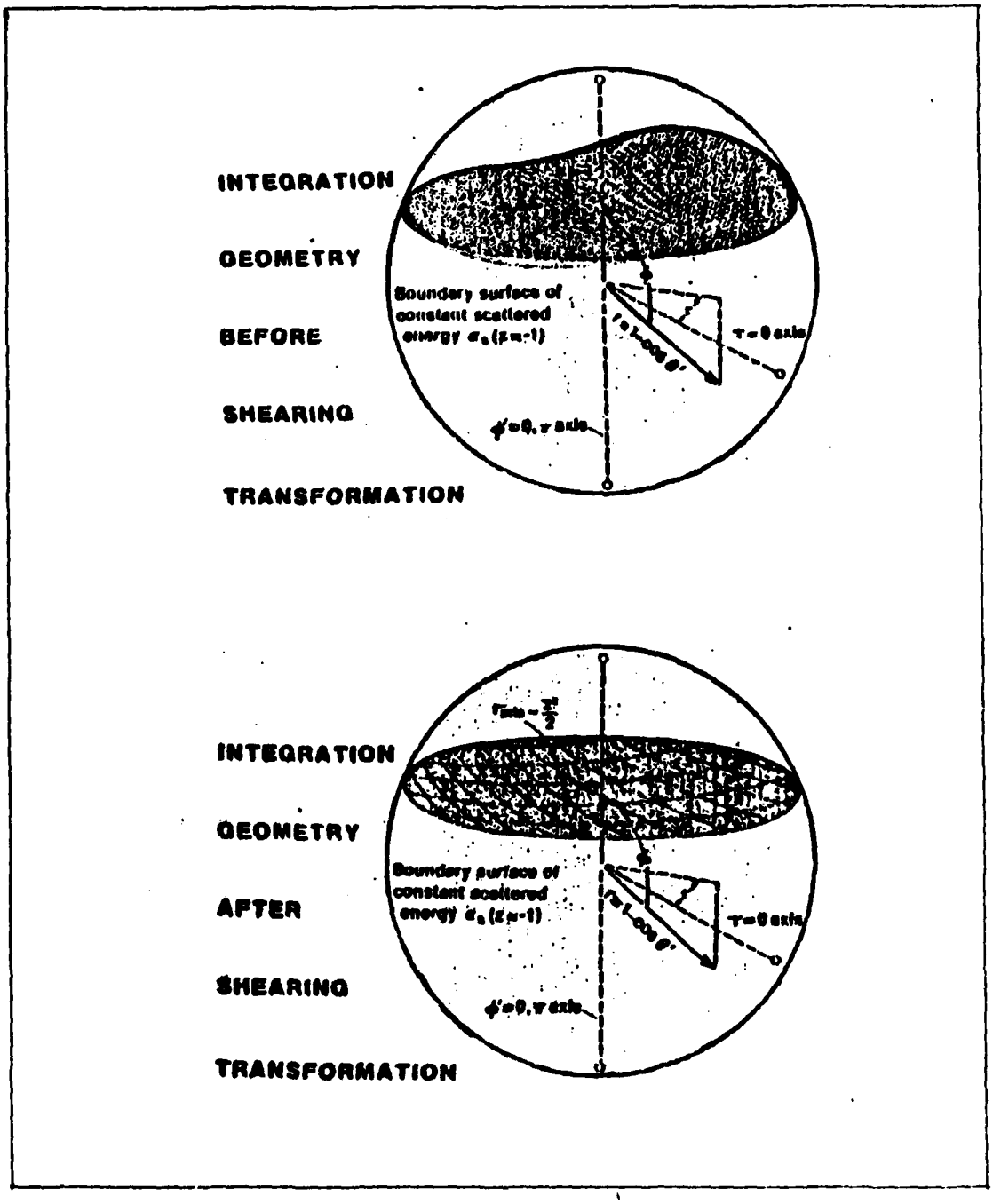

Fig. 14. Integration Geometry Prior To and After the Shearing Transformation (reprinted with permission of G. Nickel; Graphs by Douglas Weiss)

and when $z \geq 0$

$$\cos \varphi_2' = 1 \tag{35}$$

$$\cos \varphi_1' = -(3+r\xi_1)\Big/\sqrt{2r(1-\beta^2)+r^2(\beta^2-a^2)} \tag{36}$$

The final form of the cumulative distribution function can now be written. When $z<0$ the cumulative distribution function is,

$$F(3,\xi_1,a_1)=\int_{-\pi}^{\pi}\frac{d\tau}{2\pi}\int_{r_{min}}^{2}\frac{dr}{A}\int_{\varphi_1'}^{\varphi_2'}d(\cos\varphi)\left[2-2(1-\alpha')r+(1-2\alpha'+\alpha'^2)r^2\right.$$

$$\left.+\ \alpha' r^3\right]\Big/(1+\alpha' r)^3 \tag{37}$$

and for $z \geq 0$

$$F(3,\xi_1,a)=1-\left\{\int_{-\pi}^{\pi}\frac{d\tau}{2\pi}\int_{r_{min}}^{2}\frac{dr}{A}\int_{\varphi_1'}^{\varphi_2'}d(\cos\varphi)\left[2-2(1-\alpha')r+\right.\right.$$

$$\left.\left.(1-2\alpha'+\alpha'^2)r^2+\alpha' r^3\right]\Big/(1+\alpha' r)^3\right\} \tag{38}$$

An approximation can be made to further simplify the integral. For electrons and photons with kilovolt energies, $\alpha' \approx 10^{-2}$ making $\beta \approx 10^{-1}$ and 'a' on the order of 10^{-2}. Thus an 'a' can be ignored as a lowest order approximation to

equations 37 and 38. Since the α' term arises only in the Klein-Nishina formula, a numerical integration was done to determine the normalization constant when α' was small. The results were compared to analytical results obtained by ignoring α', and were in close agreement. Thus, this approximation to the scattering kernel is fairly good. The cumulative scattering probability becomes

$$F(\xi,3)=\int_{-\pi}^{\pi}\frac{d\tau}{2\pi}\int_{r_{min}}^{2}\frac{dr}{A}\int_{\varphi_1'}^{\varphi_2'}d(\cos\varphi)(2-2r+r^2) \qquad (39)$$

Further approximations yield

$$F(\xi,3)=\frac{1}{2}(\pm)h_0+3g_0+\xi g_1 \quad \begin{cases} 3<0 \\ 3\geq 0 \end{cases} \qquad (40)$$

where

$$g_n=\frac{3}{16\sqrt{2}}\int_{r_{min}}^{2}(2-2r+r^2)r^{n-1/2}dr \qquad (41)$$

and

$$h_0=\frac{3}{8}r_{min}-\frac{3}{16}r_{min}^2+\frac{1}{16}r_{min}^3 \qquad (42)$$

The cumulative scattering probability is multiplied by an electron vacancy factor $1-n(\varepsilon_{final})$ and, where ε_{final} is the final electron energy associated with a scattering event. This diminishes the probability of a scattering event occurring if the final electron state is occupied.

IV. Results

The cumulative scattering probability can be computed through the use of equations 37 and 38. A computer code was written to run on the CDC Cyber which would compute the cumulative scattering probability averaged over the velocities of an electron distribution. In addition, an electron vacancy factor was included to account for final electron energy state occupation when the gas is degenerate. The results for the cumulative scattering probability were then used to find the differential Compton cross section.

Methodology

In order to compute the cumulative scattering probability, a computer code, 'EDIST', was used to compute the one hundred equally probable velocities for an electron distribution. An incident photon energy was chosen and another program 'CSP' used the energy data from 'EDIST' to find the average cumulative scattering probability. In 'CSP', the scattered photon energy bins were first initialized. Then for each electron velocity, the probability of scattering into each energy bin was computed. The probability of scattering into a certain energy bin was multiplied by the electron vacancy factor $1-n(\epsilon)$. Just prior to computing the cumulative scattering probability, the final

electron energy necessary for a photon to scatter into a particular bin was calculated. This energy of the electron was used to compute $n(\epsilon)$. The two programs were run for cases of varying number densities, incident photon energies, and electron temperatures.

Discussion of Results

Figures 15 and 16 show the behavior of the cumulative scattering probability (equations 37 and 38) for the nondegenerate and degenerate cases. The scattered photon energy versus the probability of scattering into that energy bin is plotted for incident photon energies of 2 and 20 KeV. It can be seen that for a particular incident photon energy, the cumulative scattering probability curves shift toward higher scattered photon energies as the electron temperature is raised. This is due mainly to Doppler shifting between the electron rest frame and the lab frame. The scattered energy states accessible to the incident photon are contained in the region of the cumulative scattering probability curves where the slope is varying. In the degenerate limit, the cumulative scattering probability curves are influenced by the final energy state occupation of the electron. The curves show a decrease in the scattering probability at the higher scattered photon energies. The magnitude of this shift is a function of the electron temperature. At the higher temperatures, the degeneracy

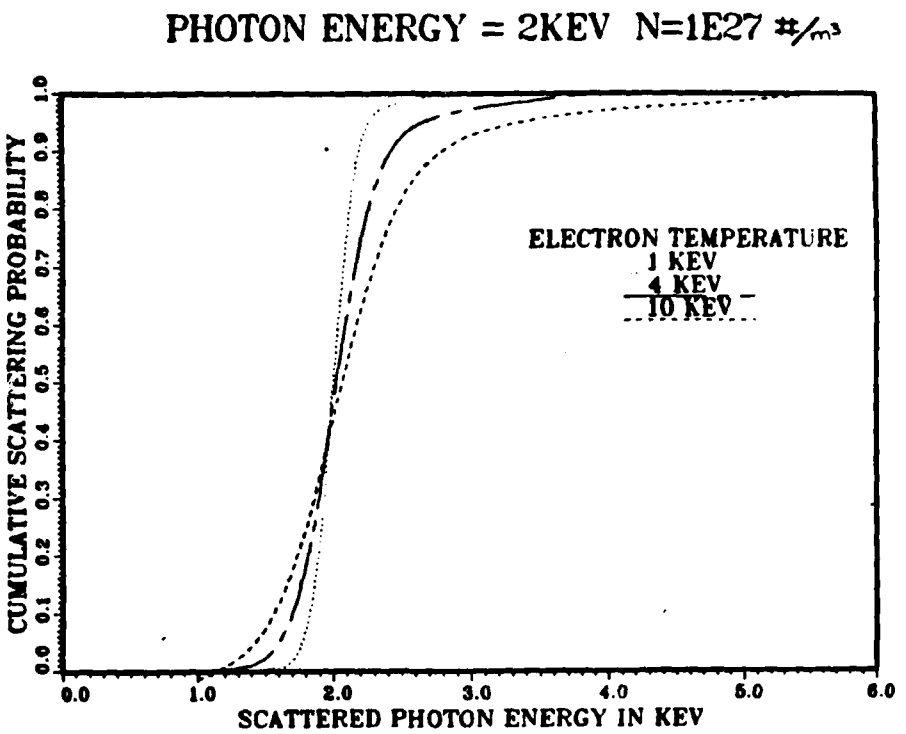

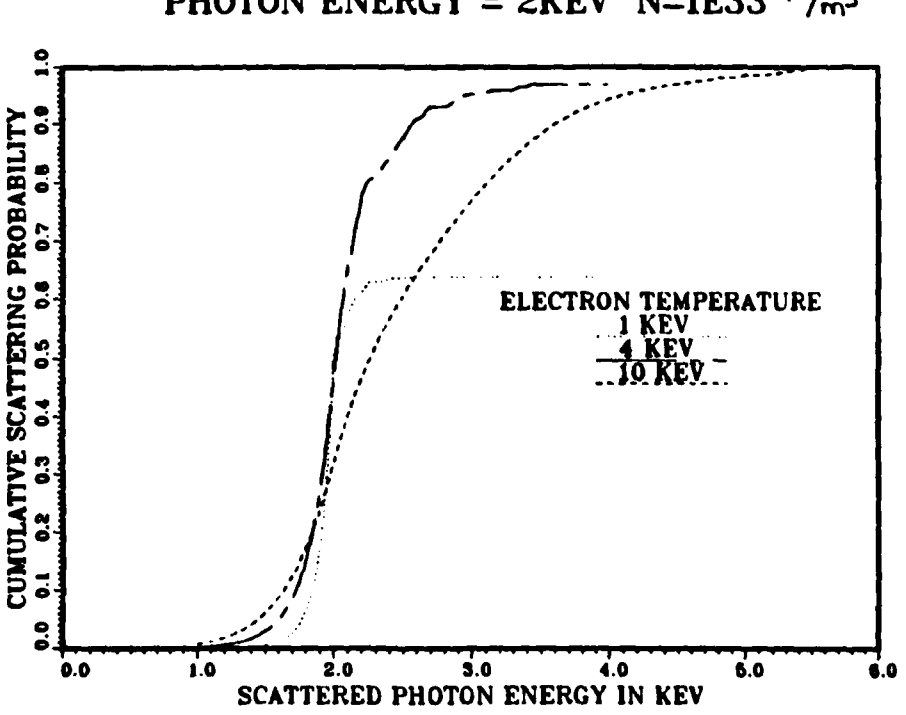

Fig. 15. Nondegenerate and Degenerate Cumulative Scattering Probabilities vs. Final Photon Energy in KeV (hv = 2 KeV)

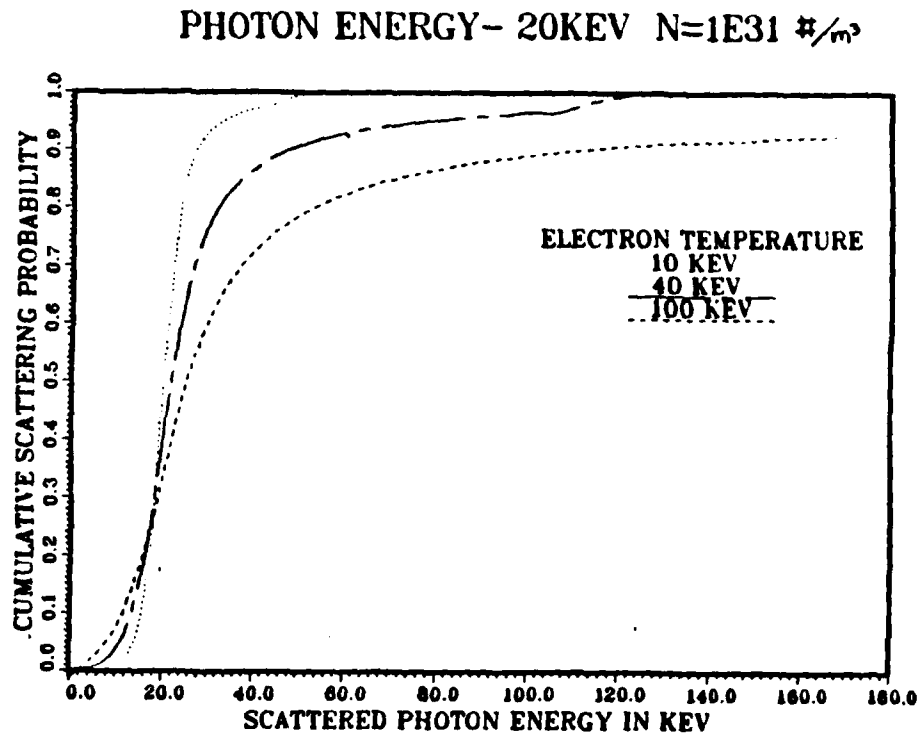

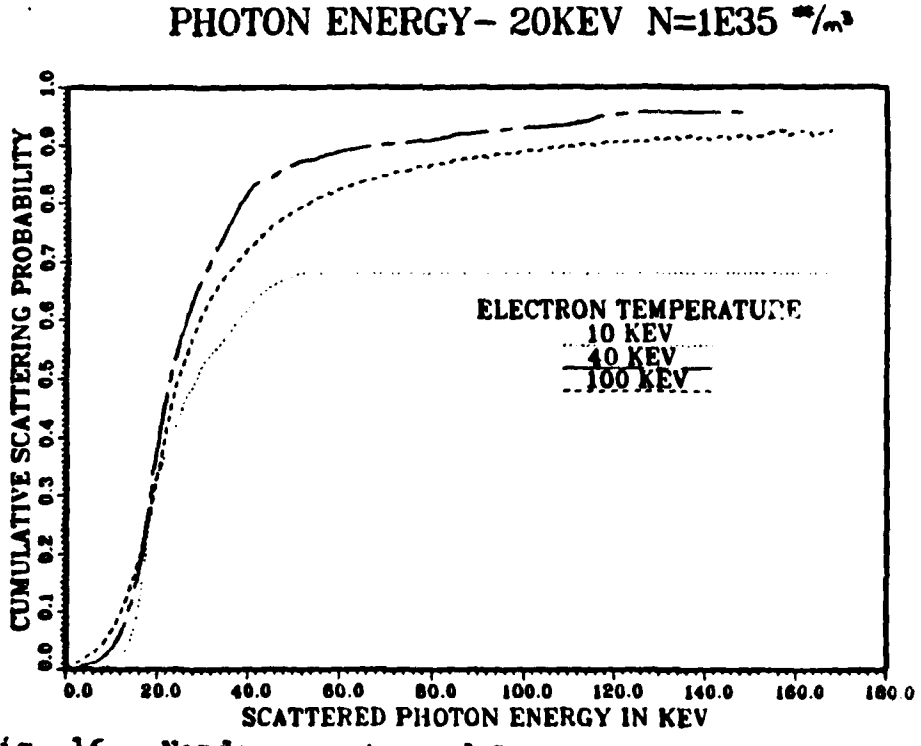

Fig. 16. Nondegenerate and Degenerate Cumulative Scattering Probabilities vs. Final Photon Energy in Kev (hv = 20 KeV)

is not as pronounced as at the low temperatures. The Compton scattering kernel can now be used to calculate Compton cross sections.

The differential Compton cross section $d(\sigma_c)$ is computed by evaluating

$$d(\sigma_c) = \sigma_{K.N.} \frac{\partial F}{\partial \alpha_s} d\alpha_s \qquad (43)$$

where $\sigma_{K.N.}$ is the Klein-Nishina cross section for small α_s,

$$\sigma_{K.N.} = \frac{8\pi}{3} r_e^2 \left(1 - 2\alpha' + \frac{26}{5}\alpha'^2 + \ldots\right) \qquad (44)$$

and $\frac{\partial F}{\partial \alpha_s}$ is the cumulative scattering probability differentiated with respect to the scattered photon energy. Since 'F' is a function of 'rmin' and 'rmin' in turn a function of α_s, explicit representation of the differentiation was tedious but not impossible. Computer runs using an averaging approach similar to that used in 'CSP' were used to compute $\frac{\partial F}{\partial \alpha_s}$. Initial results obtained proved to be inconclusive since they showed that downscatter was dominant in the Compton cross section profiles even at low incident photon energies. At low incident photon energies, the electron can be treated as being infinitely massive and the scattered photon energy is slightly shifted to lower and higher energies. This can easily be shown by evaluating the normal electron rest frame formula for Compton scattering.

Another approach was taken to compute the differential Compton cross section.

Since curves of the cumulative scattering probability versus scattered photon energy can be computed, $\frac{\partial F}{\partial \alpha_3}$ can be evaluated by finding the slope at various points on the cumulative scattering probability curves. Differential Compton cross sections were computed for electron temperatures of 1 KeV and 20 KeV, number of densities of 10^{27}, 10^{31}, 10^{33}, and 10^{35} electrons per cubic meter. Also, incident photon energies of 5, 10, 20, 40, and 60 KeV were chosen. Figures 17 and 18 show the differential cross section in millibarns per KeV versus the final scattered photon energy. The solid lines are the cross sections in the nondegenerate limit. These 'tents' show the same general behavior as results found in references (6:188) and (9:16-18).

The cross sections exhibit three distinct characteristics: Compton shift, Doppler shift, and upscatter of the photon in the lab frame. A photon will, upon scattering, have its frequency decreased due to the usual Compton shift associated with scattering of electrons at rest. This effect on the cross sections is more noticeable when the incident photon energy becomes a significant fraction of the electron rest energy. Secondly, there is broadening of the cross sections due to the Doppler effect of scattering from a distribution of moving electrons. Finally, the

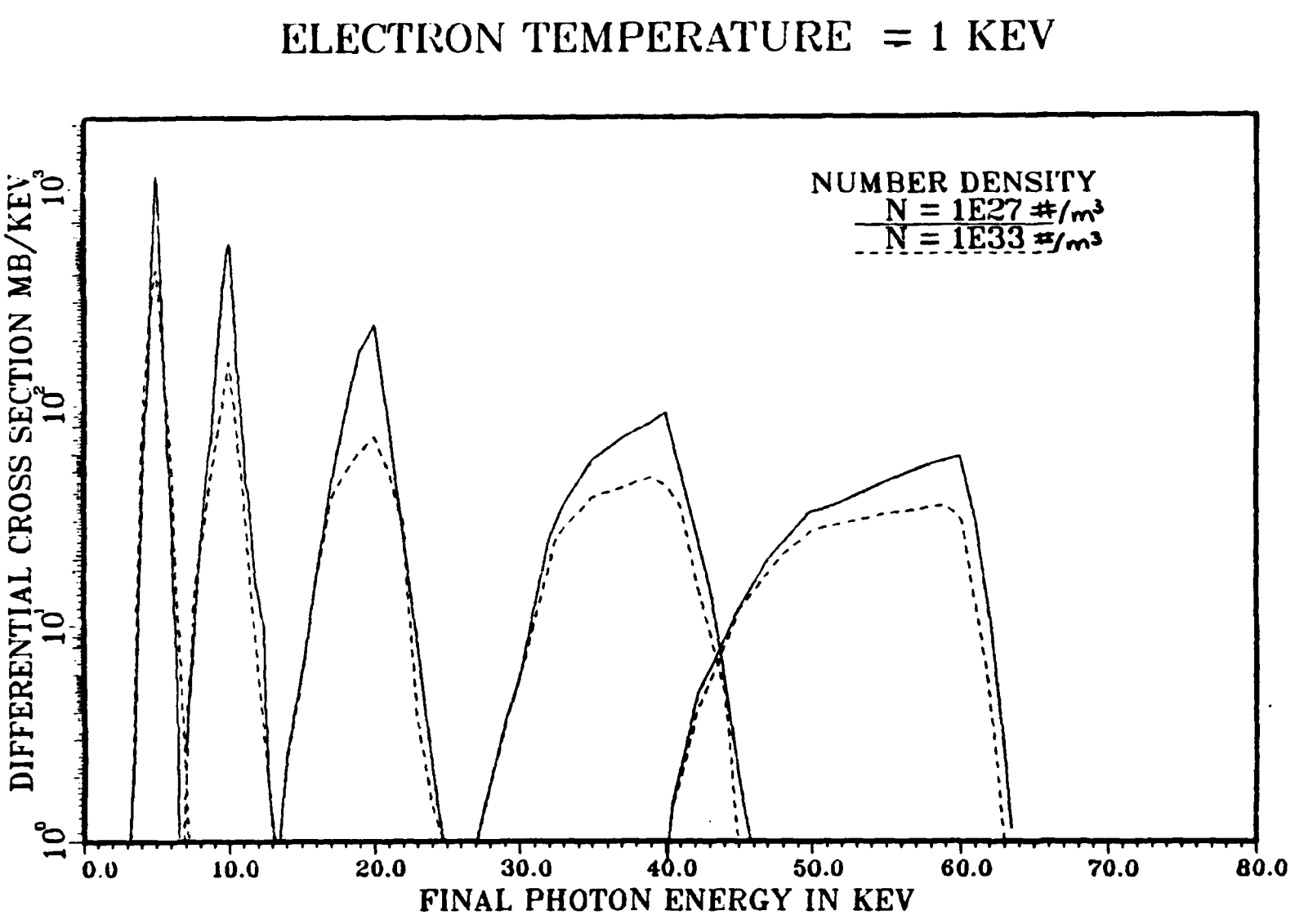

Fig. 17. Differential Cross Section vs. Final Photon Energy (kT = 1 KeV)

ELECTRON TEMPERATURE = 20 KEV

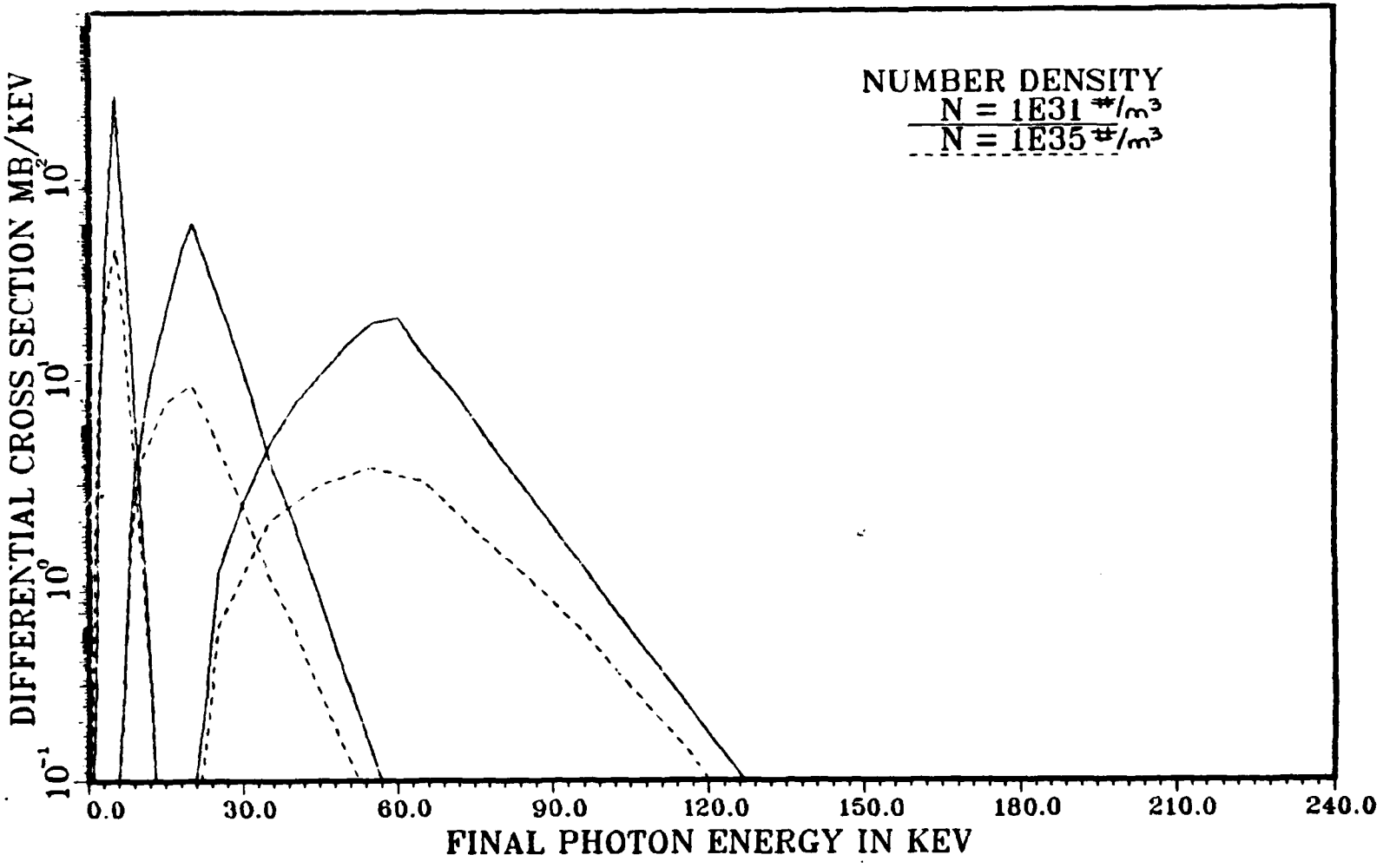

Fig. 18. Differential Cross Section vs. Final Photon Energy (kT = 20 KeV)

energy of the scattered photon will increase due to the relativistic effect that the photon will appear more intense to an electron moving toward it than away from it. This is the reason that upscatter component of the Compton cross section is seen in the lab frame even though no upscatter occurs in the rest frame. As Pomraning (9:184) points out, this blue shift is needed to balance the Compton red shift.

> If a radiation field at a certain temperature scatters from an electron gas at the same temperature, the scattered photons should have the same distribution as the incident photons [9:184].

The Compton cross sections decrease with increasing photon energy because the units are in millibarns per KeV. Thus, the cross sections fall off as one over the energy of the scattered photon. At low incident photon energies, the profile of the Compton cross sections have some characteristic width controlled by Doppler broadening. When the energy of the photon is increased, the profile of the Compton cross sections is driven by the Compton scattering formula which represents a square step function in the electron rest frame. This square step function is broadened at the higher incident photon energies and competes with and begins to dominate the Doppler effect in influencing the shape of the cross sections. Also, figure 18 shows that Doppler broadening of the Compton cross sections becomes more significant as the electron temperature is increased. The expression for $\frac{\partial F_s}{\partial \alpha_s}$ goes approximately

as $1/\beta$, so the Compton cross section for a particular incident photon energy decreases as the electron temperature is raised.

The dashed lines show the differential cross sections when the photons interact with a degenerate electron gas. The behavior is consistent with theory. The number of final energy states is limited as the gas becomes degenerate. The instances where the electron delivers most or all of its energy are decreased since the lower final energy states required for such an event are filled. If a Compton scattering event does occur, the photon will most likely downscatter to lower energies. Thus, a slight shift to lower photon energies is seen in the 'tents'. This behavior is more noticeable at higher incident photon energies. Also, the peaks of the 'tents' decrease because the cumulative scattering probability decreases in a degenerate electron gas. The general behavior of these degenerate differential Compton cross sections coincides with nondegenerate case outlined above.

A deeper appreciation of this development can be given by noting the reduction of the computational time required to evaluate the Compton cross sections. Dr. Nickel numerically evaluated equations 37 and 38 with an electron vacancy factor for the case in figure 17. His results, while agreeing with those in figure 17, took approximately an hour of CRAY time to compute. The results obtained in

this report required only 2.65 cpu seconds on the CDC Cyber.

Higher incident photon energies were not examined because the approximation to the scattering kernel breaks down as the photon energy approaches the electron rest energy. Earlier work by Nickel (7) shows that as the ratio $\frac{\alpha}{\beta}$ becomes large, the kernel becomes double valued. The breakdown in the approximation of the kernel might be alleviated by higher order approximations to equations 37 and 38. Further research is needed.

V. Recommendations

Several areas of this investigation were not fully examined but deserve further analysis. A few topics of continued research are listed below.

1. Scattering Kernel. Although the results obtained in figures 15-18 lead to good results for the Compton cross sections, it is necessary to compare these analytical results to exact ones. Therefore, numerical integration of equations 37 and 38 is needed as a yardstick to measure the accuracy of the analytical results. Also, it would be interesting to determine if higher order approximations to equations 37 and 38 lead to a better correlation with the exact results.

2. Compton Cross Sections. As mentioned in the results section, some difficulty was encountered in the explicit evaluation of the differentiated scattering kernel. It is hoped that continued work will present a clean solution to this problem.

3. Computer Implementation. An analysis should be done to find if a marked difference exists between existing codes which use the lengthy methods of determining cross sections and an updated code that used the modified

Nickel formalism. It is hoped that use of this development for Compton cross sections will drastically reduce run times and in turn save money.

VI. Conclusions

The answers obtained for Compton cross sections in the nondegenerate limit for electron and photon energies in the kilovolt regime corresponded to cross sections that exist in current literature. This showed that the computer code was running correctly and that the lowest order approximation to the Compton scattering kernel was a good one. The extension to the degenerate limit yielded Compton cross sections that were lower in magnitude and shadowed by the nondegenerate results. The degenerate results reflected the fact that lower energy states of the electron distribution were filled. Therefore, scattering to these final energy states was inhibited. The most outstanding fact of this development of angle-averaged Compton cross sections is the small amount of computer time required to obtain results. There was a decrease by three orders of magnitude in run times by using an approximation to the kernel. If further investigations of this method can be extended to photon and electron temperatures in the hundreds of KeVs and implemented into weapons or fusion computer codes, then a very significant impact on computer run times may be seen.

A. 'CSP' Listing

The program 'CSP' is used to compute the cumulative scattering probability given an initial photon energy and velocities of an electron distribution. A listing of the code and the variables is contained on the following pages.

```
      PROGRAM CSP

*
* THIS PROGRAM COMPUTES SCATTERING PROB. WITH THE
* 'NEW' RMIN FOR A DEGENERATE DISTRIBUTION
*

      INTEGER L,Q,NOD(350),TOTAL
      LOGICAL FLAG(350)
      REAL AA,BB,CC,DD,EE,FF,GG,R,TOT(350,150)
      REAL ALPHMI,ALPHMA,VI(300),NE
      REAL M,C,K,H,VOL,PI,AL(350),T,N
      REAL ALPHI,F,ALPHS,BETA,B1,LA,PROB(350)
      REAL VMAX,VMIN,DIFFER,LAPR
      PARAMETER(M=9.1E-31,C=3E8,K=1.38E-23)
      PARAMETER(H=6.63E-34,VOL=1.,PI=3.14159)

*
*    THE INCIDENT PHOTON ENERGY IS ENTERED
*

      PRINT*,'ENTER THE INCIDENT PHOTON ENERGY'
      READ*,ALPHI
      ALPHI=ALPHI/511.

*
*    THE GRID OF SCATTERED ENERGY, ALONG WITH A FLAG
*    AND COUNTER ARE INITIALIZED
*

      I=1
      DO 11 R=1,6,.0195
       AL(I)=REAL(R)/511.
      NOD(I)=1
      FLAG(I)=.TRUE.
      TOT(I,1)=0
       I=I+1
 11   CONTINUE

*
*    ENTER THE VELOCITY DATA POINTS
*

      PRINT*,'ENTER THE TOTAL # OF VELOCITY DATA POINTS'
      READ*,TOTAL

*
*    READ THE FILE "VEL" CONTAINING THE VELOCITY DATA
*
```

```
      OPEN(3,FILE='VEL')
      REWIND 3
      DO 88 I=2,TOTAL+1
        READ(3,FMT=89)VI(I)
 88    CONTINUE
 89   FORMAT(E11.3)
      CLOSE(3)

*
*    ENTER THE NUMBER DENSITY OF THE SYSTEM
*

      PRINT*,'ENTER THE NUMBER DENSITY OF THE SYSTEM'
      READ*,N

*
*    ENTER THE TEMPERATURE OF THE ELECTRONS
*

      PRINT*,'ENTER THE TEMPERATURE OF THE SYSTEM'
      READ*,T
      T=T/8.61E-8

*
*    COMPUTE CUMULATIVE SCATTERING PROBABILITY
*    CURVES FOR EACH ELECTRON VELOCITY
*

      DO 5 Q=2,TOTAL+1
      V=VI(Q)

*
*    COMPUTE ALPHA AND BETA
*

      LA=1/SQRT(1-((V/C)**2.))
      B1=1-(1/(LA**2.))
      BETA=SQRT(B1)

*
*    DETERMINE THE LIMITS OF THE SCATTERED ENERGY
*

      BB=((1/LA)+(2.*ALPHI))**2.
      AA=1+(BETA*BETA)+(2.*LA*ALPHI)
      CC=BB-((BETA*ALPHI)**2.)
      DD=CC/(LA*LA)
      EE=AA**2.
      FF=DD/EE
      GG=SQRT(1-FF)
```

```
      ALPHMA=ALPHI*(AA/CC)*(1+GG)
      ALPHMI=ALPHI*(AA/CC)*(1-GG)

*
*    COMPUTE THE PROBABILITY FOR EACH SCATTERING BIN
*

      DO 1 L=1,257

       IF (AL(L).LT.ALPHMI.OR.AL(L).GT.ALPHMA) THEN
        TOT(L,Q)=0
       ELSE
        ALPHS=AL(L)
        LAPR=ALPHI-AL(L)+LA
        CALL CHEMPO(NE,PI,VOL,M,H,K,C,LAPR,N,T)
        CALL PHOTDI(F,BETA,K,T,M,C,H,ALPHI,ALPHS,NE)
        TOT(L,Q)=F
        TOT(L,Q)=TOT(L,Q)+TOT(L,Q-1)

        IF(FLAG(L)) THEN
          NOD(L)=NOD(L)
          FLAG(L)=.FALSE.
         ELSE
          NOD(L)=NOD(L)+1
         ENDIF

        ENDIF
        PROB(L)=TOT(L,Q)/NOD(L)
 1      CONTINUE
 5      CONTINUE

*
*    WRITE OUTPUT TO THE FILE "OP"
*

      L=L-1
      OPEN(3,FILE='OP')
      REWIND 3
      WRITE(3,FMT=101)
      DO 10 I=1,L

      IF (I.NE.1) THEN
       IF (PROB(I).LT.PROB(I-1)) THEN
        PROB(I)=PROB(I-1)
       ENDIF
      ENDIF

      WRITE(3,FMT=100)AL(I)*511.,PROB(I)
 10   CONTINUE
```

```
 100     FORMAT(F7.4,5X,F7.4)
 101     FORMAT(50X)
         CLOSE(3)

         END

*****************************************************************

         SUBROUTINE PHOTDI(F,BETA,K,T,M,C,H,ALPHI,ALPHS,NE)
         REAL BETA,LAM,M,C,KT,ASQR,BESQR,ZSQR
         REAL ALPHI,ALPHS,NE
         REAL H01,H02,H03,G01,G02,G03,G04,G05,G06
         REAL G11,G12,G13,G14,G15,G16,RMIN2,RMIN3
         REAL ZESQR,A,Z,ZETA,RMIN1,RMIN,H0G0,G1,F,SRT
         LAM=1/SQRT(1-(BETA**2.))
         SRT=2.**.5

*
*    COMPUTE Z,ZETA,A
*

         Z=(1/(LAM*LAM*BETA))*((ALPHS/ALPHI)-1)
         ZETA=((ALPHS/(LAM*BETA))-BETA)
         A =ALPHS/LAM

*
*    COMPUTE RMIN
*

       ASQR=A**2.
       BESQR=BETA**2.
       ZSQR=Z**2.
       ZESQR=ZETA**2.
       IF (ASQR+ZESQR.EQ.BESQR) THEN
       RMIN=ZSQR/(2.*(1-BESQR-(ZETA*Z)))
       ELSE
       RMIN1=1-BESQR-(ZETA*Z)
       RMIN2=-BESQR+ASQR+ZESQR
       RMIN3=BESQR-1+(Z*ZETA)
       RMIN=(RMIN1-SQRT(((RMIN3)**2.)-(ZSQR*RMIN2)))/RMIN2
       ENDIF
*
*    COMPUTE G0,G1,H0
*
       H01=(3.*RMIN)/8.
       H02=(3.*RMIN*RMIN)/16.
       H03=(RMIN**3.)/16.
       H0 = H01-H02+H03

       G01=(11./20.)
       G02=SQRT(RMIN)
```

```
          G03=3./(4.*SRT)
          G04=RMIN/(4.*SRT)
          G05=(3.*RMIN*RMIN)/(40.*SRT)
          G06=G02*(G03-G04+G05)
          G0=G01-G06

          G11=(23./70.)
          G12=RMIN**1.5
          G13=1/(4.*SRT)
          G14=(3.*RMIN)/(20.*SRT)
          G15=(3.*RMIN*RMIN)/(56.*SRT)
          G16=G12*(G13-G14+G15)
          G1=G11-G16

*
*    COMPUTE F(ALPHA,ALPHAS,BETA)
*
        IF (Z.LT.0) THEN
          F=(.5-H0+(Z*G0)+(ZETA*G1))*(1.-NE)
         ELSE
          F=(.5+H0+(Z*G0)+(ZETA*G1))*(1-NE)
        ENDIF

        END

*****************************************************************
        SUBROUTINE CHEMPO(NE,PI,VOL,M,H,K,C,LAPR,N,T)
        REAL T,M,H,N,C,VOL,MU,EF,PI,KT
        REAL VOLS,NE,K,LAPR

*
*    COMPUTE FERMI ENERGY
*
        KT=K*T
        EF=(H/(M*LAPR))*(H/8.)*(((3.*N)/(PI*VOL))**(2./3.))

*
*    DETERMINE THE CHEMICAL POTENTIAL
*

        IF (((T/(EF/K))**2).GT.(12/(PI**2.))) THEN
MU=-KT*LOG((2.*VOL/N)*(((2*PI*M*LAPR*T/H)*(K/H))**1.5))
          ELSE
         MU=EF*(1-(((KT/EF)**2.)*((PI**2.)/12.)))
        ENDIF

*
*    COMPUTE THE PROBABILITY OF THE FINAL ENERGY STATE
*    BEING OCCUPIED
*
```

```
VOLS=((M*C*C*(LAPR-1))-MU)/KT
IF (VOLS.GT.87) THEN
 NE=0
ELSE
 NE=1/(EXP(VOLS)+1.)
ENDIF

END
```

Variable Listing

A = An independent variable

AA = A parameter used to compute the minimum and maximum scattered energy

AL = An array identifying the scattered energy bins

ALPHI = The incident photon energy

ALPHMA = The maximum energy a photon can scatter to when interacting with an electron of a particular speed

ALPHMI = The minimum energy a photon can scatter to when interacting with an electron of a particular speed

ALPHS = The scattered photon energy

ASQR = The variable 'A' squared

BB = A parameter used to compute the minimum and maximum scattered energy

BESQR = The variable 'BETA' squared

BETA = The speed of an electron divided by the speed of light

C = The speed of light

CC = A parameter used to compute the minimum and maximum scattered energy

DD = A parameter used to compute the minimum and maximum scattered energy

EE = A parameter used to compute the minimum and maximum scattered energy

EF = The fermi energy

F = The cumulative scattering probability equation

FF = A parameter used to compute the minimum and maximum scattered energy

FLAG = A logical flag that determines whether the scattered energy of the photon lies within the actual range of possible scattering energies

G01-G16 = Terms in the cumulative scattering probability equation

GG = A parameter used to compute the minimum and maximum scattered energy

H01-H03 = Terms in the cumulative scattering probability equation

H = Planck's constant

K = Boltzmann's constant

KT = The thermal energy of the electrons

L = A counter used to initialize the scattered energy bins

LA = One over the square root one minus beta squared

LAM = The same as variable 'LA'

LAPR = The same as 'LA' except that the electron speed in beta is that associated with the final energy of the scattered electron

M = The mass of an electron

MU = The chemical potential

N = The number of density of the electrons

NE = The probability of occupation of an electron state

NOD = An array used to identify the number of times the scattering probability was computed for each scattering bin

PI = The constant 'pi'

PROB = An array that divides 'TOT' by 'NOD'

Q = A counter variable

R = A counter variable

RMIN = The variable 'Rmin'

RMIN1 = A parameter used to compute 'RMIN'

RMIN2 = A parameter used to compute 'RMIN'

RMIN3 = A parameter used to compute 'RMIN'

T = The equilibrium temperature of the electrons

TOTAL = The total number of velocity data points

TOT = An array that contains the scattering probability at different scattered energy bins

VI = An array containing the velocities associated with the electron distribution

VOL = The volume of the system of electrons and photons

VOLS = A parameter used to determine if the exponential term in the occupation equation is too large and prevents overflow errors.

Z = An independent variable

ZETA = An independent variable

ZESQR = The variable 'ZETA' squared

ZSQR = The variable 'Z' squared

B. 'EDIST' Listing

The computer code 'EDIST' computes the velocity distribution data needed in the program 'CSP'. This data is then used to find the cumulative scattering probability averaged over these velocities. A code and variable listing are contained in this appendix.

```
      PROGRAM EDIST
*
* GIVEN # DENSITY AND TEMP, THIS PROGRAM DIVIDES THE DIST.
* INTO 100 EQUALLY PROBABLE SECTIONS.  THE ENERGIES
* ASSOCIATED WITH THE EQUAL PROBABLE BLOCKS ARE USED TO
* COMPUTE THE SCATTERING PROBABILITY CURVES.
*
      REAL F(10000),EKT,E,DE,B,A,CONST,EN(200)
      REAL VI(200),CSQR,NU,MU,W
      INTEGER N,L
      CSQR=3E8*3E8
      PRINT*,'ENTER THE TEMPERATURE OF THE ELECTRONS'
      READ*,EKT
      PRINT*,'ENTER THE NUMBER DENSITY OF THE SYSTEM'
      READ*,NU
      DE=EKT/1000.
      E=DE
      CALL CHEMPO(MU,NU,EKT,E)
      MU=MU/1.602E-16
      W=(E-MU)/EKT

      IF (W.GT.87) THEN
       B=0
      ELSE
       B=SQRT(E*(E+1022.))*(E*511.)*(1/(EXP(W)+1))
      ENDIF

      F(1)=.5*DE*B
      A=B
      DO 1 N=2,10000
       E=E+DE
      CALL CHEMPO(MU,NU,EKT,E)
      MU=MU/1.602E-16
      W=(E-MU)/EKT

      IF (W.GT.87) THEN
      B=0
      ELSE
       B=SQRT(E*(E+1022.))*(E+511.)*(1/(EXP(W)+1))
      ENDIF

      F(N)=F(N-1)+.5*DE*(B+A)
      A=B
1     CONTINUE
      CONST=F(10000)+B*EKT
      PRINT*,EKT,CONST

      F(1)=F(1)/CONST
      DO 5 N=2,10000
```

```
        F(N)=F(N)/CONST
 5      CONTINUE

*
*     WRITE THE EQUALLY PROBABLE VELOCITIES TO THE
*     FILE "VEL"
*

        OPEN(3,FILE='VEL')
        REWIND 3
        DO 20 I=1,L-1
         VI(I)=SQRT(CSQR*(1-(1/(EN(I)/511.+1))**2.))
         WRITE (3,FMT=100)VI(I)
 20     CONTINUE
 100    FORMAT(E11.3)
        CLOSE(3)
*
*     WRITE THE ELECTRON PROBABILITIES TO THE
*     FILE "MIKE"
*

        OPEN(3,FILE='MIKE')
        REWIND 3
        DO 55 I=1,L-1
         WRITE (3,FMT=101)F(I)
 55     CONTINUE
 101    FORMAT(E11.3)
         WRITE (3,FMT=102)CONST
 102      FORMAT(E13.4)
        CLOSE(3)

        END


*****************************************************************
        SUBROUTINE CHEMPO(MU,NU,EKT,E)
        REAL T,M,H,NU,C,VOL,MU,EF,PI,KT,LAM,K
        PARAMETER(C=3.E8,M=9.1E-31,H=6.63E-34,VOL=1)
        PARAMETER(K=1.38E-23,PI=3.14159)
        T=EKT/8.61E-8
        LAM=(E/511.)+1

*
*       COMPUTE FERMI ENERGY
*
        KT=K*T
        EF=(H/(M*LAM))*(H/8.)*(((3.*NU)/(PI*VOL))**(2./3.))

*
```

```
*        DETERMINE THE CHEMICAL POTENTIAL
*

          IF (((T/(EF/K))**2).GT.(12/(PI**2.))) THEN
MU=-KT*LOG((2.*VOL/NU)*(((2*PI*M*LAM*T/H)*(K/H))**1.5))
            ELSE
           MU=EF*(1-(((KT/EF)**2.)*((PI**2.)/12.)))
           ENDIF

          END
```

Variable Listing

A = The value of the electron distribution at a particular energy, and used as the left boundary in the trapezoidal integration

B = Same as 'A', but used as the right boundary in the trapezoidal integration

BETA = The speed of an electron divided by the speed of light

C = The speed of light

CONST = The numerically determined normalization constant

CSQR = The variable 'C' squared

DE = The energy increments used to integrate the distribution

E = The energy of an electron in the distribution

EF = The fermi energy

EN = The array which contains the hundred equally probable energies of the electron distribution

EKT = Same as 'KT', the thermal energy of the electrons

F = An array which contains the values of the electron distribution at various energies

H = Planck's constant

K = Boltzmann's constant

KT = The thermal energy of the electrons

LAM = The same as variable 'LA'

M = The mass of an electron

MU = The chemical potential

N = The number density of the electrons

NE = The probability of occupation of an electron state

PI = The constant 'pi'

T = The equilibrium temperature of the electrons

VI = The array containing the velocities associated with the electron distribution

VOL = The volume of the system of electrons and photons

W = A parameter used to determine if the exponential term in the occupation equation is too large and prevents overflow errors

C. Derivation of the Chemical Potential

The chemical potential is derived for the cases when $\frac{\mu}{kT}$ is less and greater than zero. The case where $\frac{\mu}{kT} > \emptyset$ is addressed first. The equation that defines the chemical potential is the distribution of the electrons integrated over all possible momentum. This is equal to the number of electrons in the system.

$$N = \int_0^\infty \frac{8\pi V}{h^3} \frac{p^2}{e^{(\epsilon(p)-\mu)/kT}+1} dp \qquad (C-1)$$

For ease of calculation, a variable change is made. Let

$$p = \sqrt{2m_o\epsilon} \qquad (C-2)$$

$$dp = \sqrt{\frac{m_o}{2\epsilon}}\, d\epsilon \qquad (C-3)$$

the density is now,

$$\rho = a \int_0^\infty \frac{\epsilon^{1/2}\, d\epsilon}{e^{(\epsilon-\mu)/kT}+1} \qquad (C-4)$$

where 'a' is equal to

$$\frac{g 4\pi (2m_o)^{3/2}}{h^3} \qquad (C-5)$$

Next define f(e) as

$$a\varepsilon^{1/2}. \qquad (C-6)$$

and using a hint from reference (2:36), the integral can be rewritten.

$$\rho=\int_0^\infty \frac{f(\epsilon)d\epsilon}{e^{(\epsilon-\mu)/kT}+1}=\int_\mu^\infty \frac{f(\epsilon)d\epsilon}{e^{(\epsilon-\mu)/kT}+1}+\int_0^\mu f(\epsilon)d\epsilon+\int_0^\mu \frac{f(\epsilon)d\epsilon}{e^{(\mu-\epsilon)/kT}+1} \qquad (C-7)$$

A variable change is made in the first integral. Letting $x=\frac{(\epsilon-\mu)}{kT}$ and changing the limits the first integral becomes,

$$\int_0^\infty \frac{f(\mu+xkT)}{e^x+1}\,kTdx \qquad (C-8)$$

Similarly for the third integral let $x=\frac{-(\epsilon-\mu)}{kT}$ and the limits are changed such that the integral becomes,

$$\int_0^{\beta\mu} \frac{f(\mu-xkT)}{e^x+1}\,kTdx \qquad (C-9)$$

thus,

$$\rho=\int_0^\infty \frac{f(\mu+xkT)}{e^x+1}\,kTdx+\int_0^{\beta\mu} \frac{f(\mu-xkT)}{e^x+1}\,kTdx+\int_0^\mu f(\epsilon)d\epsilon \qquad (C-10)$$

In the limit where $T_f \gg T$ ($\beta\mu \approx \infty$) so that integrals one and three can be gathered under the same limits.

$$\rho = \int_0^{\infty} \frac{f(\mu + xkT) + f(\mu - xkT)}{e^x + 1} \, kT\,dx + \int_0^{\mu} f(\epsilon)\,d\epsilon \qquad (C\text{-}11)$$

A Taylor series expansion is then performed about μ. The density is now

$$\rho = \int_0^{\mu} f(\epsilon)\,d\epsilon + \frac{\pi^2}{6} kT^2 f'(\mu) + \frac{7\pi^4}{360} kT^4 f'''(\mu) + H.O.T. \qquad (C\text{-}12)$$

After substituting

$$f'(\mu) = \frac{a}{2} \mu^{-1/2} \qquad (C\text{-}13)$$

$$f'''(\mu) = a \frac{3}{8} \mu^{-5/2} \qquad (C\text{-}14)$$

into equation C-12 and evaluating the remaining integral the chemical potential is,

$$\mu = \epsilon_f \left[1 - \frac{\pi^2}{12} \left(\frac{kT}{\mu} \right)^2 + \frac{\pi^4}{720} \left(\frac{kT}{\mu} \right)^4 \right] \qquad (C\text{-}15)$$

where ϵ_f is the fermi energy and defined as

$$\epsilon_f = \frac{h^2}{8 m_0} \left(\frac{3N}{\pi V} \right)^{2/3} \qquad (C\text{-}16)$$

Further approximations lead to

$$\mu = \epsilon_f \left[1 - \frac{\pi^2}{12} \left(\frac{T}{T_f} \right)^2 + \frac{\pi^4}{720} \left(\frac{T}{T_f} \right)^4 \right] \qquad (C\text{-}17)$$

where

T_f = The Fermi temperature

Since the approximation made was for large $\frac{\mu}{kT}$, equation (C-17) is valid until μ is zero.

In the nondegenerate limit ($\mu<0$), the energy eigenvalues possible for single particle are,

$$\varepsilon = \frac{\pi^2 h^2}{2\pi V^{2/3}} (n_x^2 + n_y^2 + n_z^2) \qquad (C-18)$$

and the partition function for a single particle in a monatomic gas is

$$Z_1 = \sum_{\text{STATES}} e^{-\beta \varepsilon_i} = \sum_{n_x} \sum_{n_y} \sum_{n_z} e^{-\delta_0 (n_x^2 + n_y^2 + n_z^2)} \qquad (C-19)$$

where $\delta_0 = \frac{\pi^2 h^2}{2\pi V^{2/3}}$ and n_x, n_y, and n_z can vary from 1 to ∞

so
$$Z_1 = \sum_{n_x=1}^{\infty} e^{-\delta_0 n_x^2} \sum_{n_y=1}^{\infty} e^{-\delta_0 n_y^2} \sum_{n_z=1}^{\infty} e^{-\delta_0 n_z^2} \qquad (C-20)$$

$$Z_1 = Z_x Z_y Z_z$$

The approximation that the number of energy states is a continuum allows for the replacement of the summation symbol by an integral so that

$$Z_x = \int_0^{\infty} e^{-\delta_0 n_x^2} d n_x = \frac{1}{2} \left(\frac{\pi}{\delta_0} \right)^{1/2} \qquad (C-21)$$

thus

$$Z_1 = g\left(\frac{kTm_o}{2\pi^2\hbar^2}\right)V \qquad (C\text{-}22)$$

where 'g' has been added to account for the spin degeneracy. For a system of 'N' indistinguishable particles the partition function (11:155) is,

$$Z = \frac{Z_1^N}{N!} \quad \text{OR} \quad Z = \frac{g^N V^N \left(\frac{m_o kT}{2\pi\hbar^2}\right)^{3N/2}}{N!} \qquad (C\text{-}23)$$

Taking the natural logarithm of both sides yields

$$\log Z = N\left[\log(gV) + \tfrac{3}{2}\log(kT) + \tfrac{3}{2}\log\left(\frac{m_o}{2\pi\hbar^2}\right)\right] - \log N! \qquad (C\text{-}24)$$

using Stirling's theorem (10:611) which states

$$\log N! = N\log N - N \qquad (C\text{-}25)$$

further simplifies equation (C-24) to

$$\log Z = \left[\log\left(\frac{gV}{N}\right) - \tfrac{3}{2}\log\left(\frac{1}{kT}\right) + \tfrac{3}{2}\log\left(\frac{m_o}{2\pi\hbar^2}\right)\right] + 1 \qquad (C\text{-}26)$$

Now, by definition (10:323)

$$\mu = -kT\left(\frac{\partial \log Z}{\partial N}\right)_{V,T} \qquad (C\text{-}27)$$

so that the chemical potential in the nondegenerate limit is,

$$\mu = -kT \log \left[\frac{g}{N} V \left(\frac{m_o kT}{2\pi\hbar^2} \right)^{3/2} \right] \qquad (C\text{-}28)$$

D. Derivation of the Equation 13

Development of the Compton scattering formula with an angular dependence in the laboratory reference frame is important for determining the limits for the scattered photon distribution. The approach requires that transformations and rotations be made to simplify the final expression.

Starting in the lab frame, the velocity of the electron is chosen to be in the direction of the z-axis and making an angle of φ with the incident photon.

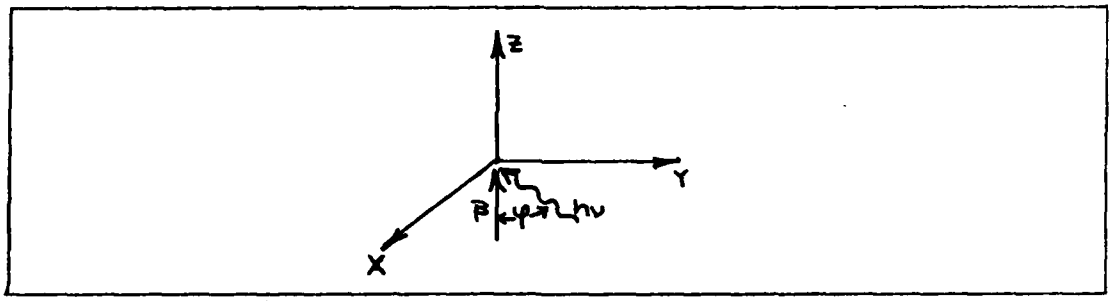

The photon 4 vector is,

$$P_\nu = \frac{h\nu}{c} \begin{bmatrix} \sin\varphi\cos\chi \\ \sin\varphi\sin\chi \\ \cos\varphi \\ 1 \end{bmatrix} \qquad (D-1)$$

where χ is an arbitrary angle chosen for convenience.

The electron 4 vector is

$$P_e = \begin{bmatrix} 0 \\ 0 \\ m_o c\sqrt{\gamma^2-1} \\ m_o c\,\gamma \end{bmatrix} \qquad (D-2)$$

Next, the symmetrized and normalized lorentz transformation matrix

$$L = \begin{bmatrix} 1 & 0 & 0 & 0 \\ 0 & 1 & 0 & 0 \\ 0 & 0 & \gamma & -\gamma\beta \\ 0 & 0 & -\gamma\beta & \gamma \end{bmatrix} \qquad (D-3)$$

is used to transform both electron and photon vectors to the electron rest frame. Under the transformation these vectors become,

$$P_\nu' = \frac{h\nu}{c}\begin{bmatrix} \sin\varphi\cos\chi \\ \sin\varphi\sin\chi \\ \gamma\cos\varphi - \gamma\beta \\ -\gamma\beta\cos\varphi + \gamma \end{bmatrix} (D-4); \quad P_e' = m_o c\begin{bmatrix} 0 \\ 0 \\ 0 \\ 1 \end{bmatrix} (D-5)$$

Next, the coordinate system is rotated to remove the 'x' and 'y' components in the photon 4 vector. For ease of computation, values of 1 and 0 were chosen for cos χ and sin χ respectively. Thus,

$$P_\nu' = \frac{h\nu}{c}\begin{bmatrix} \sin\varphi \\ 0 \\ \gamma(\cos\varphi - \beta) \\ \gamma(1 - \beta\cos\varphi) \end{bmatrix} \qquad (D-6)$$

A rotation about the 'y' axis is done using the rotation matrix

$$R = \begin{bmatrix} \cos\delta & 0 & -\sin\delta & 0 \\ 0 & 1 & 0 & 0 \\ -\sin\delta & 0 & \cos\delta & 0 \\ 0 & 0 & 0 & 0 \end{bmatrix} \quad (D-7)$$

and the rotated photon 4 vector becomes

$$h\nu \begin{bmatrix} \sin\varphi\cos\delta - \gamma(\cos\varphi-\beta)\sin\delta \\ 0 \\ \sin\varphi\sin\delta + \gamma(\cos\varphi-\beta)\cos\delta \\ \gamma(1-\beta\cos\varphi) \end{bmatrix} \quad (D-8)$$

The angle δ is picked so that the 'x' component is zero. This requires that

$$\sin\varphi\cos\delta = \gamma(\cos\varphi-\beta)\sin\delta \quad (D-9)$$

and from this sin δ and cos δ are

$$\sin\delta = \frac{\sin\varphi}{\gamma(1-\beta\cos\varphi)} \quad (D-10)$$

$$\cos\delta = \frac{\gamma(\cos\varphi-\beta)}{\gamma(1-\beta\cos\varphi)} \quad (D-11)$$

so the photon 4 vector is now,

$$h\nu \begin{bmatrix} 0 \\ 0 \\ \gamma(1-\beta\cos\varphi) \\ \gamma(1-\beta\cos\varphi) \end{bmatrix} \qquad (D-12)$$

Using the above results, Compton scattering in the electron rest frame becomes,

$$h\nu'' = \frac{\gamma(1-\beta\cos\varphi)\, h\nu}{1+\gamma(1-\beta\cos\varphi)(1-\cos\theta)\frac{h\nu}{m_0c^2}} \qquad (D-13)$$

The scattered photon 4 vector is

$$\frac{h\nu''}{c} \begin{bmatrix} \sin\vartheta\cos\tau \\ \sin\vartheta\sin\tau \\ \cos\vartheta \\ 1 \end{bmatrix} \qquad (D-14)$$

where θ and τ are the polar and azimuthal angles in the electron rest frame. Next, a reverse rotation transformation is done to get,

$$\frac{h\nu''}{c} \begin{bmatrix} \sin\vartheta\cos\tau\cos\delta + \cos\vartheta\sin\delta \\ \sin\vartheta\sin\tau \\ -\sin\vartheta\cos\tau\sin\delta + \cos\vartheta\sin\delta \\ 1 \end{bmatrix} \qquad (D-15)$$

or

$$\frac{h\nu''}{c}\begin{vmatrix} \left[\sin\vartheta\cos\tau\,\gamma(\cos\varphi-\beta)+\cos\vartheta\sin\varphi\right]/\gamma(1-\beta\cos\varphi) \\ \sin\vartheta\sin\tau \\ \left[\sin\vartheta\cos\tau\sin\varphi+\cos\vartheta\,\gamma(\cos\varphi-\beta)\right]/\gamma(1-\beta\cos\varphi) \\ 1 \end{vmatrix} \quad (D\text{-}16)$$

Finally, the inverse of the initial lorentz transform is used to transform to the lab frame. The momentum is

$$\frac{h\nu_s}{c} = \frac{h\nu''}{c}\left\{\frac{\gamma\beta}{\gamma(1-\beta\cos\varphi)}\left[\gamma\cos\vartheta(\cos\varphi-\beta)-\sin\vartheta\cos\tau\sin\varphi\right]+\gamma\right\} \quad (D\text{-}17)$$

Substituting the equation D-13 into D-17 and dividing both sides by mc yields,

$$\frac{\alpha_s}{\alpha} = \frac{\gamma^2(1-\beta\cos\varphi)+\beta\gamma^2\cos\vartheta(\cos\varphi-\beta)+\beta\gamma\sin\vartheta\sin\tau\sin\varphi}{1+\gamma(1-\beta\cos\varphi)(1-\cos\vartheta)\alpha} \quad (D\text{-}18)$$

Where the change in the origin of τ changes $\cos\tau$ to $\sin\tau$. This is equation 13. This work was done largely by Dr. Nickel (7) and was presented to give a deeper appreciation of the origin of equation 13.

E. Derivation of the Relativistic Fermi Distribution

When the temperature of a system becomes large enough the distribution of electrons can no longer be described by equation 3. An expression for relativistic fermi distributions is derived to characterize this region. First, begin with the distribution of electrons when the gas is nonrelativistic.

$$f(p) = \frac{8\pi V}{h^3} \frac{p^2 dp}{e^{(\varepsilon(p)-\mu)/kT} + 1} \qquad (E-1)$$

Next, replace momentum and energy with the relativistic equivalents

$$\varepsilon = m_o c^2 (\gamma - 1) \qquad (E-2)$$

$$p = m_o v \gamma \qquad (E-3)$$

The distribution function in terms of velocity is

$$f(v) = \frac{8\pi V m_o^3}{h^3} \frac{v^2 \gamma^5 dv}{e^{(m_o c^2(\gamma-1)-\mu)/kT} + 1} \qquad (E-4)$$

But, V is a function of velocity so using the substitutions

$$v^2 = \frac{\gamma^2 - 1}{\gamma^2} c^2 \qquad (E\text{-}5)$$

$$dv = \frac{c}{\gamma^2} \frac{d\gamma}{\sqrt{\gamma^2 - 1}} \qquad (E\text{-}6)$$

the distribution of electrons becomes,

$$f(\gamma)d\gamma = \frac{8\pi V}{h^3} m_0^3 c^3 \frac{\gamma(\gamma^2-1)}{\sqrt{\gamma^2-1}} \frac{d\gamma}{e^{(m_0c^2(\gamma-1)-\mu)/kT}+1} \qquad (E\text{-}7)$$

Integrating (E-7) from one to infinity yields the total number of electrons in the system.

$$N = \int_1^\infty \frac{8\pi V}{h^3} (m_0 c)^3 \frac{\gamma\sqrt{\gamma^2-1}\, d\gamma}{e^{(m_0c^2(\gamma-1)-\mu)/kT}+1} \qquad (E\text{-}8)$$

Bibliography

1. Eisberg, Robert and Robert Resnick. Quantum Physics of Atoms, Molecules, Solids, Nuclei, and Particles. New York: Wiley and Sons, 1974.

2. Feynmann, Richard P. Statistical Mechanics. Reading MA: W. A. Benjamin, Inc., 1972.

3. Jackson, E. Atlee. Equilibrium Statistical Mechanics. Englewood Cliffs NJ: Prentice-Hall, Inc., 1968.

4. Motz, H. The Physics of Laser Fusion. New York: Academic Press, 1979.

5. Nickel, George H. "Angle-Averaged Compton Cross Sections," Second International Conference and Workshop on Radiative Properties on Hot Dense Matter.

6. Nickel, George H. A simple Approximation to the Energy Distribution of Compton Scattered Photons, 21 August 1981.

7. Nickel, George H. Personal correspondence. Los Alamos National Laboratory, Los Alamos NM, 14 December 1984.

8. Nickel, George H. Telephone interview. Los Alamos National Laboratory, Los Alamos NM, 14 December 1984.

9. Pomraning, G. C. The Equations of Radiation Hydrodynamics. New York: Pergamon Press, 1973.

10. Reif, F. Fundamentals of Statistical and Thermal Physics. New York: McGraw-Hill Book Co., 1965.

11. Rosser, W. G. V. An Introduction to Statistical Physics. Chichester BG: Ellis Horgood Limited, 1982.

VITA

Joseph M. Pochkowski was born on the 27th of November, 1961 at Subic Bay Naval Station, Philippine Islands. He graduated from Frank W. Cox High School in 1979 and went on to receive a Bachelor of Science degree in Engineering Physics from the University of Tennessee. He was commissioned through the AFROTC program and assigned to the Air Force Institute of Technology Graduate Nuclear Engineering program. He is a member of Tau Beta Pi and Sigma Pi Sigma.

Permanent address: 111 Carnegie Drive
Oak Ridge, Tennessee 37830

UNCLASSIFIED

SECURITY CLASSIFICATION OF THIS PAGE

REPORT DOCUMENTATION PAGE

1a. REPORT SECURITY CLASSIFICATION UNCLASSIFIED	1b. RESTRICTIVE MARKINGS
2a. SECURITY CLASSIFICATION AUTHORITY	3. DISTRIBUTION/AVAILABILITY OF REPORT Approved for public release; distribution unlimited.
2b. DECLASSIFICATION/DOWNGRADING SCHEDULE	
4. PERFORMING ORGANIZATION REPORT NUMBER(S) AFIT/GNE/ENP/85M-17	5. MONITORING ORGANIZATION REPORT NUMBER(S)
6a. NAME OF PERFORMING ORGANIZATION School of Engineering 6b. OFFICE SYMBOL (If applicable) AFIT/EN	7a. NAME OF MONITORING ORGANIZATION
6c. ADDRESS (City, State and ZIP Code) Air Force Institute of Technolgy Wright-Patterson Air Force Base, OH 45433	7b. ADDRESS (City, State and ZIP Code)
8a. NAME OF FUNDING/SPONSORING ORGANIZATION 8b. OFFICE SYMBOL (If applicable)	9. PROCUREMENT INSTRUMENT IDENTIFICATION NUMBER
8c. ADDRESS (City, State and ZIP Code)	10. SOURCE OF FUNDING NOS. PROGRAM ELEMENT NO. / PROJECT NO. / TASK NO. / WORK UNIT NO.
11. TITLE (Include Security Classification) See Box 19	
12. PERSONAL AUTHOR(S) Joseph M. Pochkowski, B.S., 2Lt, USAF	
13a. TYPE OF REPORT MS Thesis 13b. TIME COVERED FROM _____ TO _____	14. DATE OF REPORT (Yr., Mo., Day) 1985 March 15. PAGE COUNT 75
16. SUPPLEMENTARY NOTATION	

17. COSATI CODES		
FIELD	GROUP	SUB. GR.
20	10	
18	01	

18. SUBJECT TERMS (Continue on reverse if necessary and identify by block number)
Compton Scattering, Plasma, Radiation Transport, Cross sections, Electron Gas,

19. ABSTRACT (Continue on reverse if necessary and identify by block number)

Title: Angle Averaged Compton Cross Sections for Degenerate Electron Gases

Thesis Chairman: Lt Col William F. Bailey,

Approved for public release: IAW AFR 190-17.
17 April 85
LYNN E. WOLAVER
Dean for Research and Professional Development
Air Force Institute of Technology (ATC)
Wright-Patterson AFB OH 45433

20. DISTRIBUTION/AVAILABILITY OF ABSTRACT UNCLASSIFIED/UNLIMITED ☒ SAME AS RPT. ☐ DTIC USERS ☐	21. ABSTRACT SECURITY CLASSIFICATION UNCLASSIFIED
22a. NAME OF RESPONSIBLE INDIVIDUAL Lt Col William F. Bailey	22b. TELEPHONE NUMBER (Include Area Code) (513) 255-4498 22c. OFFICE SYMBOL AFIT/ENP

DD FORM 1473, 83 APR EDITION OF 1 JAN 73 IS OBSOLETE.

UNCLASSIFED

SECURITY CLASSIFICATION OF THIS PAGE

Compton scattering in dense electron gases is reviewed. The processes of Compton scattering are incorporated into the development of an analytic expression for the scattering kernel. The kernel is good for electron and photon energies in the KeV regime.
The kernel is in turn used to compute angle averaged differential Compton cross sections. The development of this analytic expression for the kernel leads to a decrease of three orders of magnitude in the computational times for the Compton cross sections.

→ cant keywords include? see [illegible]

END

FILMED

6-85

DTIC